PNL-2638
UC-80

The Impact of a Hanford Nuclear Energy Center on Cloudiness and Insolation

J. V. Ramsdell

July 1978

Prepared for the U.S. Department of Energy
under Contract No. EY-76-C-06-1830

Pacific Northwest Laboratory
Operated for the U.S. Department of Energy
by

Battelle
Memorial Institute

PNL-2638

NOTICE

PACIFIC NORTHWEST LABORATORY
operated by
BATTELLE
for the
UNITED STATES DEPARTMENT OF ENERGY
Under Contract EY-76-C-06-1830

Printed in the United States of America
Available from
National Technical Information Service
United States Department of Commerce
5285 Port Royal Road
Springfield, Virginia 22151

Price: Printed Copy $____*; Microfiche $3.00

*Pages	NTIS Selling Price
001-025	$4.00
026-050	$4.50
051-075	$5.25
076-100	$6.00
101-125	$6.50
126-150	$7.25
151-175	$8.00
176-200	$9.00
201-225	$9.25
226-250	$9.50
251-275	$10.75
276-300	$11.00

PNL-2638
UC-80

THE IMPACT OF A HANFORD NUCLEAR ENERGY CENTER ON CLOUDINESS AND INSOLATION

J. V. Ramsdell

July 1978

Prepared for the U.S. Department of Energy under Contract No. EY-76-C-06-1830

Pacific Northwest Laboratory
Richland, Washington 99352

CONTENTS

FIGURES

TABLES

THE IMPACT OF A HANFORD NUCLEAR ENERGY CENTER ON CLOUDINESS AND INSOLATION

J. V. Ramsdell

Pacific Northwest Laboratory
Richland, Washington

INTRODUCTION

Reactor cooling system effluents could, under some conditions, contribute to an increase in cloudiness and a decrease in insolation (solar radiation received at the earth's surface). This report presents the results of an evaluation of the potential impact of a Hanford Nuclear Energy Center (HNEC) on cloudiness and insolation. It is one of a series of reports prepared by the Pacific Northwest Laboratory (PNL) in the course of an evaluation of the energy center concept as it might be applied to the Department of Energy is Hanford Area in Washington State[1-3]. Previous topical reports in the series deal with a variety of subjects including electrical transmission[4], fuel cycle[5], heat disposal[6-8], and reliability of generation[9-10].

The energy center concept involves the grouping of a large number of power plants at a common site. An energy center may also include fuel production and waste disposal facilities. Typically the number of power plants considered ranges from 10 to 40. In the conceptual evaluation of a Hanford Nuclear Energy Center both 20 and 40 generating unit centers have been considered, with the 20 unit center receiving the most attention. Within an energy center the individual power plants are generally grouped in clusters of about 4.

Thermal power plants cooling systems ultimately release a significant amount of energy to the atmosphere. In current designs this energy is primarily released as latent heat of evaporation of water and sensible heat in the form of

increased air temperature. Both the addition of water and the increase in temperature can contribute to the formation of clouds by increasing the instability of the atmosphere and triggering natural cloud formation processes. The additional water vapor may also contribute to the formation of clouds by directly bringing the air to saturation.

Increasing the cloudiness will, in turn, alter the balance of short wave (solar) and long wave (terrestrial) radiation. An increased cloud layer will increase the fraction of incoming solar radiation reflected prior to reaching the surface. Some of the reflected solar radiation will reach the surface as diffuse radiation and some will be lost to space. The increased cloudiness will also absorb an increased fraction of the long wave terrestrial radiation. Much of this energy is reradiated toward earth and is thereby retained in the earth-atmosphere system.

Specifically this report estimates the change in sky cover and the resulting change in solar radiation. It does not attempt to distinguish between direct and diffuse solar radiation, and it does not deal with the impact of increased cloudiness on long wave radiation.

The report is divided into four sections. In the first section we will develop the approach followed in the study, starting from estimation of the distributions of cooling system effluents, proceeding through estimation of changes in sky cover, and ending with estimation in changes in insolation. In the second section we will briefly describe the HNEC and discuss the aspects of the climatology of the Hanford Area that relate to sky cover and solar radiation. We will then develop the specific relationships required to make actual estimates of the changes. In the final sections we will examine

the estimated changes, compare them with worst case estimates, discuss their statistical significance, and discuss the conclusions reached.

CONCEPTUAL DEVELOPMENT

Estimating changes in sky cover and solar radiation is a complex problem. If approached rigorously as a time varying, three dimensional problem in atmospheric diffusion and transport, thermodynamics and radiative transfer, it would require resources beyond those currently available. Therefore, we approach the problem in a series of steps, each of which is treated with simplified "back of the envelope" models. Frequently it is necessary to resort to use of probability arguments.

Sky cover is one of the variables included in standard weather observations. It is the fraction of the sky covered by clouds and is expressed in tenths. The amount of sky cover reported is a subjective estimate of the observer and not the result of a precise measurement. Sky cover observations include the estimated or measured height of each cloud layer. A ceiling is said to exist when the total sky cover is 6/10 or greater. Some weather observations also include cloud types. The cooling system effluents from an HNEC might alter any or all of these cloud characteristics. In this study we will concentrate on estimating the change in the total sky cover. However, in the process of estimating these changes we will postulate certain, limited changes in cloud height and type.

Changes in sky cover are potentially related to a number of factors including: wind direction and speed, atmospheric stability, air temperature and humidity profile, the magnitude and distribution of the cooling system effluent releases, the time of day and year, and the initial sky cover. To a large extent the sky cover change will be a function of the magnitude

of the perturbation in atmospheric humidity and stability caused by the combined effluents from the cooling systems. The form of the change will be affected by atmospheric stability, temperature and humidity, and the location of the change will be a function of wind direction and geometric configuration of the source. Finally the increase in total sky cover cannot exceed fraction of the sky that is clear.

Our basic approach is to first treat the problem of atmospheric diffusion and transport of cooling system effluents to identify the location where changes are most likely, and to estimate the magnitude of the atmospheric perturbation caused by the effluents. This is done using a multiple-source, sector-average, Gaussian diffusion model. We will then use the estimated magnitude of the perturbations at each location in the effluent plume to estimate the fractional increase in sky cover at the location. Finally we will use the probability of occurrence of the modeled atmospheric conditions (wind direction, wind speed and atmospheric stability), and the fractional increase in sky cover to modify the climatological sky cover probability distribution. The climatological distribution of sky cover is assumed to represent current conditions in the entire area and is therefore independent of position, but the revised sky cover probability distribution is a function of position. The revised sky cover distribution is then used to estimate the change in insolation at each location.

The undepleted insolation passing through a plane normal to the sun's rays at the top of the earth's atmosphere is about 1.95 ly min^{-1} (cal/cm^2-min). This is called the solar constant. The solar energy reaching the earth's surface is a function of latitude, time of year and day, cloudiness and air quality. Usually the energy flux is significantly less than the solar constant. However, occasionally the combination of direct radiation and radiation reflected from clouds can cause the energy flux at the surface to approach the solar constant

for short periods. The effect of cloudiness on solar radiation depends on a number of factors including, the amount of sky cover, cloud types, and cloud height. There are several types of solar radiation measurements, however the most common is measurement of total incoming short-wave radiation received on a horizontal surface at the earth's surface. This measurement does not distinguish between direct and diffuse radiation.

To estimate the changes in solar radiation resulting from increased sky cover, we will make use of the revised sky cover probability distribution and empirical relationships between sky cover and solar radiation. These relationships, developed using insolation data collected at Hanford, provide an estimate of the solar radiation that would be expected at each location based on the revised cloud distribution. The decrease in insolation can then be estimated by comparing current climatological average values with those estimated from the revised cloudiness distribution.

We will now develop each of these concepts in detail.

The Diffusion Model

The multiple-source diffusion model used in this study was developed for an earlier HNEC study and is described in detail in Reference (8). It is a sector-average, Gaussian model that incorporates reflection at the surface and at an optional upper boundary. Individual sources are treated as virtual-point sources, and the concentration at each receptor point is estimated by combination of the concentrations from all sources. The sector-average model is described in Section 3.3 of Meteorology and Atomic Energy - 1968[11], while the treatment of the reflecting lid is based upon Section 6.6 of Csanady's Turbulent Diffusion in the Environment[12].

For purposes of this study we will use water as an indicator of the modification potential of the cooling system

effluents. A large increase in atmospheric water content is assumed to correspond to a high potential for increasing sky cover. However, we do not claim that the modification will be caused by any specific process, i.e., saturation or triggering an instability.

The model used to estimate increases in water content (assumed to be water vapor) is:

$$(\Delta\rho_v)_{ki} = \frac{Q_i\hat{n}}{(2\pi)^{3/2}\sigma_z\bar{u}x} \sum_{j=-\infty}^{\infty} \left\{ \exp\left[\frac{(z-h_i+2jH)^2}{-2\sigma_z^2}\right] + \exp\left[\frac{(z+h_i+2jH)^2}{-2\sigma_z^2}\right] \right\} \qquad (1)$$

where:

$(\Delta\rho_v)_{ki}$	is the increase in water vapor concentration at receptor k due to source i,
Q_i	is the water vapor release rate of source i,
$\hat{n}$	is related to the assumed plume width, ϕ_o, by $\hat{n} = \pi/\phi_o$ when ϕ_o is the radians,
σ_z	is the vertical dispersion parameter,
$\bar{u}$	is the wind speed,
x	is the distance between the receptor and virtual point source,
z	is the height above the ground,
h_i	is the effective height for source i, and
H	is the height of the reflecting lid.

Equation 1 can be simplified if any or all of z, h_i and H are zero. The greatest simplification occurs if H is zero. In that case the infinite sum is eliminated. If h_i is zero the two exponential terms can be combined. If z=o the infinite sum is twice the sum from o to ∞. Finally, if all three are zero, the infinite sum and the exponential terms are eliminated.

In the current application none of these simplifications is appropriate, but the infinite sum is truncated at j=±2.

In the case of cooling tower effluents the effective height of release is the actual release height plus plume rise due to buoyancy. Brigg's formulae are used to estimate final plume rise[13].

In model computations, the Briggs' formulations[14] for σ_z are used. Table 1 gives the Hanford stability classes used, the corresponding Pasquill-Gifford stability classes, and the Briggs' σ_z formulations.

TABLE 1. Relationships Between σ_z, Atmospheric Stability and Distance from the Virtual Point Source to Receptor

Stability Class		σ_z
Pasquill-Gifford	Hanford	
A		$.20x$
B	Unstable	$.12x$
C		$.08x/(1+.0002x)^{1/2}$
D	Neutral	$.06x/(1+.0015x)^{1/2}$
E	Slightly stable	$.03x/(1+.0003x)$
F	Moderately stable	$.02x/(1+.0003x)$
G		$.012x/(1+.0003x)$

During high wind speed conditions, a standard wake correction is applied to the values of σ_z.

The Sky Cover Model

In the current application, the diffusion model is run for each combination of wind speed, direction and atmospheric stability. At the completion of each run the increase in water content is used to estimate the increase in cloudiness as a

function of position. The climatological change in sky cover is estimated by summing the results for each combination of wind speed, direction and stability weighted by frequency of occurrence of the combination. For this initial study we assume that sky cover is statistically independent of these factors. If a more detailed study is warranted, the statistical independence will be examined and taken into account as necessary.

The relationship between the cooling system effluents and increased cloudiness are not well established. A number of studies, e.g., References (15) through (17), have used numerical models to predict the extent clouds and plumes produced by cooling towers. In general these models require more input data than is readily available for an HNEC. In addition, the models' abilities to adequately handle the synergistic effects of multiple effluent sources are open to question. As a result, we will treat the relationship between effluent concentration and increased cloudiness in a highly parameterized fashion. We will assume that an increase in water content at a point is directly related to a fractional increase in cloudiness. The relationship will be entered in the sky cover model as a table. As better information becomes available, the table can be altered and more realistic relationships can be formulated.

If we let SC represent the sky cover, the amount of the sky available for increased cloudiness is (10-SC). The increase in sky cover is then the product of the sky available and the fractional increase, f_i, resulting from a given cooling system effluent concentration, i.e.,

$$\Delta SC^* = f_i(10-SC) \quad . \qquad (2)$$

And, the estimate of the corresponding sky cover assuming an operating HNEC, SC* is

$$SC^* = SC + f_i(10-SC) \quad . \tag{3}$$

We will assume that the sky cover observations at the Hanford Meteorology Station are representative of the whole Mid-Columbia Region so that SC is not a function of position. However, the fractional increase in sky cover is a function of position. Therefore, SC* is also a function of position.

We will treat the temporal variation of average sky cover by use of probability distributions for SC. These distributions will be changed on a monthly basis. Systematic diurnal variations in sky cover exist, but in the Mid-Columbia region they are small compared to the annual variation represented by the monthly probability distributions. As a result, they will be neglected.

It seems reasonable to assume that the relationship between cooling system effluent concentration and fractional increase in sky cover should have both annual and diurnal variability. Because of the limited information on which to base this relationship, we will neglect any diurnal variations and treat the annual variations by altering the conversion table seasonally. In the winter we will allow a relatively small increase in water content to make a relatively large fractional increase in sky cover; in the summer a relatively large increase in water content will make a relatively small fractional increase in sky cover, and the spring and fall will be treated in an intermediate manner. We will examine the sensitivity of the sky cover model to changes in the conversion table by modeling each season with a "worst case table" in which a small increase in water content results in an overcast sky condition.

After the change in sky cover is estimated at each position, the sky cover probability distribution at each position will be updated. If we let $P_o(SC)$ be the climatological probability of sky cover, SC, and P_w be the joint probability of the given wind speed and direction, and atmospheric stability, the change in

sky cover probability ΔP_{SC} is :

$$\Delta P_{SC} = P_o(SC) P_w \quad . \tag{4}$$

We then update the sky cover probability distributions at each position using SC and SC* as indices:

$$P^*_{ij}(SC^*) = P^*_{ij}(SC^*) + \Delta P_{SC} \tag{5}$$

and

$$P^*_{ij}(SC) = P^*_{ij}(SC) - \Delta P_{SC} \tag{6}$$

where $P^*_{ij}(SC^*)$ and $P^*_{ij}(SC)$ are updated parts of the sky cover probability distribution at position i,j. Prior to the first update, $P^*_{ij}(SC)$ are set equal to $P_o(SC)$; as the number of conditions modeled increases they take on their own characteristics.

When all atmospheric conditions have been modeled, we compute a new mean sky cover for each position using Equation (7):

$$\overline{SC^*}_{ij} = \sum_{SC^*} SC^* \; P^*_{ij}(SC^*) \quad . \tag{7}$$

The initial average sky cover is computed using SC and $P_o(SC)$. Finally we estimate the increase in sky cover as:

$$\Delta \overline{SC}_{ij} = \overline{SC^*}_{ij} - \overline{SC} \quad . \tag{8}$$

The outputs of the sky cover model are, then: an updated probability distribution of sky cover, an estimate of the average sky cover assuming an operating HNEC, and an estimate

of the increase in average sky cover over its current climatological value. Each of these items varies from month to month.

The Solar Radiation Model

The literature on the relationship between sky cover and solar radiation is relatively extensive and much of it is applicable to the current problem. Geiger[18] indicates that the ratio of solar radiation on clear days to that on cloudy days is about .25 in the winter, .50 in the summer, and has an annual average about .40. More recent works[19-23] give quantitative relationships between sky cover and radiation. In general there relationships show a quadratic decrease in radiation with increasing sky cover. A wide range of numerical constants in the relationships indicates that the equations are rather specific to the particular data set used in their development. As a result we will use solar radiation and sky cover data from Hanford to develop our own relationship.

The literature (e.g., 20, 24-27) clearly shows that, in addition to total sky cover, cloud type is a significant factor in determining the reduction in solar radiation. In particular high, thin cirriform clouds are significantly less effective in reducing solar radiation than are lower, thicker clouds. The use of total sky cover, including cirriform clouds in estimating solar radiation tends to underestimate in solar radiation[20,25]. Lund[24], and Lund and Shanklin[26] indicate that the probability seeing the sun is 6 to 20% greater than the probability of a cloud-free line of sight. The difference is largely a result of cirriform clouds. Finally Angell and Korshover[27] indicate that high, thin cirrus clouds have no effect on sunshine. As a result, our treatment of the sky cover probability distribution will distinguish between sky and low ceilings. High ceilings will be treated as cirriform clouds.

We will estimate the solar radiation at any time during operation of an HNEC as the product of the solar radiation in the absence of the HNEC and a function that relates sky cover and solar radiation at Hanford. That is:

$$SR^*_{ij} = SR_o \, F(SC^*, \overline{SC}) \tag{9}$$

where SR^*_{ij} is an estimate of the solar radiation at i,j given sky cover SC*; SR_o is the average solar radiation and $F(SC^*, \overline{SC})$ relates solar radiation and sky cover.

The average solar radiation for a given period of time is found by weighting the estimates of the past HNEC solar radiation by the probability of SC*. This is shown in Equation (10):

$$\overline{SR^*_{ij}} = \overline{SR}_o \sum_{SC^*} F(SC^*, \overline{SC}) P^*_{ij}(SC^*) \tag{10}$$

where $\overline{SR}_o$ is the appropriate pre-HNEC average. The decrease in solar radiation is then simply the difference between $\overline{SR^*_{ij}}$ and $\overline{SR}_o$.

Prior to developing the table that specifically relates cooling system effluent concentration to increased sky cover and a mathematical expression for $F(SC^*, \overline{SC})$, we will discuss the HNEC configuration and the Hanford area climate.

THE HANFORD NUCLEAR ENERGY CENTER

The conceptual HNEC configuration and the climatology of the Hanford area are important because the results presented are specific to the HNEC, although the approach described is general.

HNEC Configuration

The Hanford area is situated in the southern portion of Eastern Washington near the Oregon border as shown in Figure 1. The Columbia River, which runs through the area, provides an adequate source of water for the operation of wet cooling systems in the center.

During the HNEC conceptual studies numerous sites have been considered as potential cluster locations. Analysis of the HNEC concept is currently concentrating on a 20 power plant center with clusters located at sites 1 through 5 in Figure 2. In this report, HNEC specifically refers to power plant clusters at these locations. Each cluster consists of four power plants that are assumed to use mechanical draft towers for cooling.

In the computations, the cooling systems for the power plants in each cluster are treated as a single entity; no effort has been made to examine small scale effects. When a cluster is to be the effluent source, a virtual point source is found using wind direction, stability and an actual source width of 1609 m (1 mi.). It is assumed that each cluster will occupy approximately 2.6 Km^2 (1 sq. mi.). The height of the cooling towers is assumed to be 25 m. Receptors are treated as points. A detailed discussion of the source-receptor geometry is contained in Reference 8.

Hanford Diffusion Climatology

The basic reference on Hanford Climatology is Climatography of the Hanford Area[28]. Additional information relative to the conceptual HNEC is given in Reference 8. In general, the climate is typical of a mid-latitude desert-steppe. The prevailing wind directions are northwest and southwest, with speeds averaging between 2 and 3 m s^{-1} and occasional periods of high speeds.

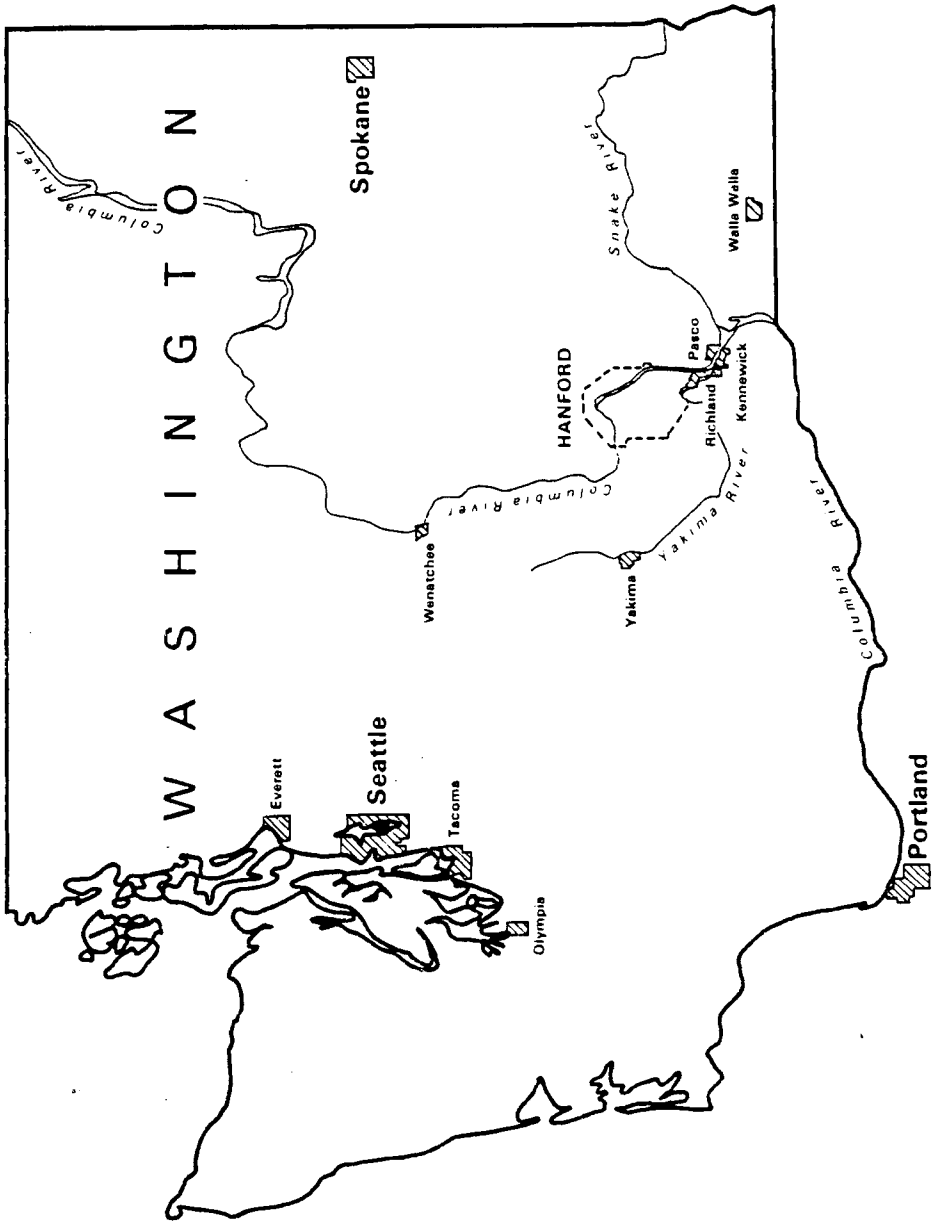

FIGURE 1. The Location of the Department of Energy's Hanford Area.

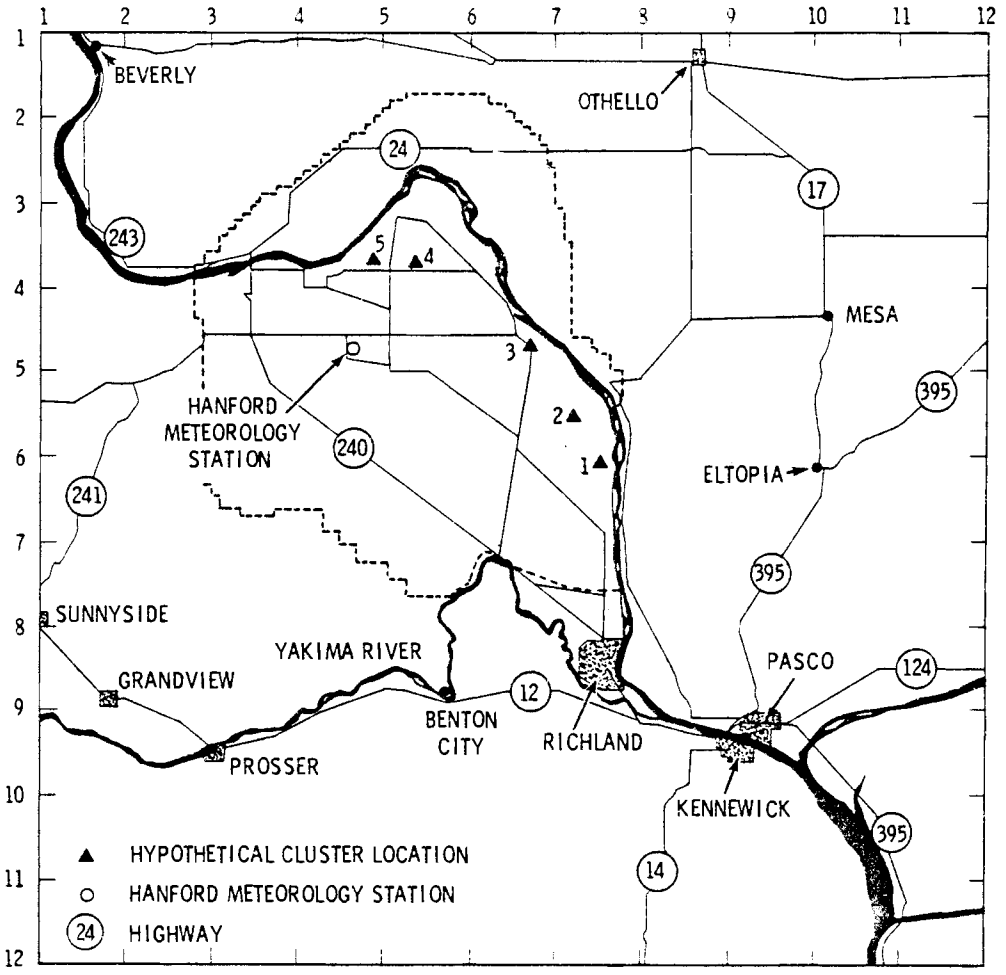

FIGURE 2. The Mid Columbia Area and Potential Cluster Locations for an HNEC. Grid Spacing is 8000 M.

Atmospheric diffusion is related to wind and atmospheric stability as shown in Equation (1). The joint frequency distributions of wind direction, wind speed and atmospheric stability required for diffusion computations involving specific sources and receptors are given in Tables 2-5 for Hanford by season.

TABLE 2. Spring Percentage Frequency Distribution of Wind Speed and Wind Direction at 200-Foot Level vs. Atmospheric Stability

		NNE	NE	ENE	E	ESE	SE	SSE	S	SSW	SW	WSW	W	WNW	NW	NNW	N	VAR.	CALM	TOTAL
0 - 3	VS	0.05	0.03	0.01	0.04	0.05	0.05	0.03	0.03	0.03	0.03	0.03	0.10	0.06	0.06	0.08	0.05	0.05	0.05	0.82
	MS	0.16	0.20	0.13	0.14	0.26	0.29	0.18	0.16	0.17	0.22	0.16	0.38	0.27	0.32	0.31	0.27	0.16	0.22	3.99
	N	0.28	0.42	0.29	0.34	0.32	0.32	0.09	0.18	0.13	0.17	0.10	0.22	0.16	0.28	0.36	0.46	0.35	0.11	4.59
	U	0.35	0.50	0.24	0.31	0.23	0.26	0.12	0.11	0.10	0.08	0.07	0.10	0.09	0.18	0.20	0.44	0.31	0.02	3.72
4 - 7	VS	0.01	0.01	0.01	0.	0.04	0.06	0.04	0.04	0.07	0.12	0.12	0.20	0.22	0.19	0.11	0.05	0.	0.	1.28
	MS	0.18	0.16	0.13	0.21	0.28	0.45	0.26	0.32	0.27	0.34	0.56	1.03	1.03	1.05	0.62	0.44	0.02	0.	7.35
	N	0.33	0.39	0.31	0.38	0.28	0.51	0.26	0.34	0.27	0.36	0.33	0.40	0.52	0.73	0.59	0.55	0.08	0.	6.63
	U	0.78	0.81	0.52	0.46	0.41	0.58	0.39	0.42	0.38	0.44	0.26	0.27	0.36	0.82	0.78	0.90	0.17	0.	8.74
8 -12	VS	0.01	0.01	0.00	0.	0.00	0.04	0.06	0.02	0.01	0.05	0.13	0.20	0.28	0.59	0.13	0.02	0.	0.	1.54
	MS	0.16	0.19	0.16	0.13	0.13	0.27	0.31	0.21	0.26	0.42	0.96	1.95	2.95	1.81	0.61	0.27	0.	0.	10.78
	N	0.24	0.16	0.10	0.11	0.10	0.15	0.18	0.21	0.39	0.52	0.54	0.61	0.84	0.97	0.27	0.27	0.	0.	5.66
	U	0.43	0.37	0.15	0.11	0.09	0.23	0.21	0.20	0.40	0.55	0.46	0.27	0.52	1.07	0.41	0.43	0.00	0.	5.91
13-18	VS	0.	0.	0.	0.00	0.	0.01	0.03	0.	0.01	0.00	0.05	0.11	0.26	0.70	0.07	0.01	0.	0.	1.25
	MS	0.10	0.07	0.05	0.07	0.02	0.12	0.26	0.09	0.14	0.46	1.15	1.66	3.68	2.23	0.21	0.18	0.	0.	10.49
	N	0.19	0.08	0.03	0.01	0.01	0.05	0.11	0.17	0.32	0.60	0.83	0.81	1.25	0.95	0.06	0.10	0.	0.	5.59
	U	0.35	0.18	0.04	0.02	0.00	0.03	0.06	0.09	0.29	0.62	0.70	0.28	0.70	0.91	0.11	0.20	0.	0.	4.59
19-24	VS	0.	0.	0.	0.	0.	0.00	0.01	0.01	0.	0.	0.	0.01	0.05	0.14	0.01	0.	0.	0.	0.22
	MS	0.02	0.01	0.01	0.02	0.	0.02	0.07	0.05	0.11	0.28	0.47	0.23	1.27	0.96	0.02	0.01	0.	0.	3.54
	N	0.08	0.04	0.01	0.	0.00	0.03	0.05	0.09	0.25	0.58	0.66	0.33	1.09	0.87	0.02	0.04	0.	0.	4.14
	U	0.09	0.05	0.01	0.01	0.	0.	0.01	0.04	0.19	0.48	0.55	0.18	0.47	0.69	0.02	0.03	0.	0.	2.81
OVER 24	VS	0.	0.	0.	0.	0.	0.	0.	0.	0.	0.01	0.00	0.	0.	0.00	0.	0.	0.	0.	0.01
	MS	0.01	0.01	0.	0.	0.	0.	0.	0.02	0.08	0.18	0.11	0.02	0.34	0.33	0.	0.01	0.	0.	1.11
	N	0.02	0.01	0.00	0.00	0.	0.	0.01	0.04	0.20	0.63	0.41	0.08	0.66	0.76	0.00	0.00	0.	0.	2.84
	U	0.01	0.03	0.02	0.	0.	0.	0.	0.01	0.14	0.71	0.47	0.13	0.33	0.57	0.00	0.00	0.	0.	2.42
TOTALS	VS	0.07	0.05	0.03	0.04	0.09	0.16	0.17	0.10	0.12	0.21	0.33	0.62	0.86	1.68	0.39	0.12	0.05	0.05	5.13
	MS	0.62	0.63	0.47	0.57	0.70	1.15	1.07	0.85	1.03	1.90	3.41	5.28	9.53	6.71	1.76	1.16	0.18	0.22	37.25
	N	1.15	1.10	0.75	0.84	0.71	1.06	0.69	1.03	1.57	2.86	2.88	2.45	4.53	4.55	1.31	1.42	0.43	0.11	29.43
	U	2.02	1.93	0.98	0.91	0.74	1.10	0.78	0.87	1.49	2.89	2.52	1.23	2.47	4.22	1.53	2.00	0.48	0.02	28.18

TABLE 3. Summer Percentage Frequency Distribution of Wind Speed and Wind Direction at 200-Foot Level vs. Atmospheric Stability

		NNE	NE	ENE	E	ESE	SE	SSE	S	SSW	SW	WSW	W	WNW	NW	NNW	N	VAR	CALM	TOTAL
0 - 3	VS	0,02	0,01	0,	0,01	0,00	0,02	0,01	0,02	0,01	0,03	0,03	0,03	0,04	0,03	0,01	0,02	0,01	0,01	0,31
	MS	0,10	0,09	0,07	0,09	0,10	0,15	0,07	0,10	0,08	0,12	0,16	0,25	0,20	0.24	0,12	0,16	0,10	0,10	2,28
	N	0,17	0,28	0,20	0,24	0,25	0,27	0,09	0,19	0,11	0,17	0,12	0,17	0,14	0.19	0,25	0,30	0,41	0,08	3,63
	U	0,36	0,47	0,20	0,24	0.26	0,30	0,18	0,21	0.12	0,20	0,16	0,17	0,12	0.27	0,22	0,43	0,61	0,03	4,55
4 - 7	VS	0,01	0,01	0,01	0,01	0,01	0,02	0,03	0,03	0,01	0,04	0,08	0,17	0,16	0.09	0,06	0,03	0,00	0,	0,76
	MS	0,17	0,15	0,12	0,15	0,20	0,30	0,18	0,17	0,17	0,31	0,43	0,93	0,86	0.63	0,44	0,21	0,04	0,	5,46
	N	0,38	0,40	0,25	0,34	0,41	0,54	0,29	0,36	0,30	0,41	0,40	0,48	0,46	0.67	0,55	0,55	0,20	0,	7,00
	U	1,32	1,28	0,74	0,89	0,72	0,91	0,56	0,73	0,72	0,80	0,59	0,64	0,61	1,21	1,08	1,38	0,67	0,	14,86
8 -12	VS	0,	0,01	0,	0,	0,01	0,01	0,01	0,02	0,01	0,02	0,08	0,23	0,33	0.42	0,17	0,02	0,	0,	1,33
	MS	0,20	0,20	0,10	0,14	0,19	0,16	0,22	0,11	0,09	0,26	0,77	1,93	2,98	1.43	0,37	0,23	0,	0,	9,38
	N	0,21	0,14	0,07	0,08	0,11	0,11	0,09	0,07	0,17	0,46	0,57	0,65	0,78	0.84	0,22	0,19	0,	0,	4,77
	U	0,66	0,49	0,20	0,18	0,15	0,20	0,13	0,18	0,42	0,86	0,75	0,42	0,73	1.47	0,52	0,55	0,01	0,	7,91
13-18	VS	0,	0,	0,	0,	0,	0,00	0,01	0,	0,01	0,01	0,02	0,05	0,23	0.86	0,07	0,	0,	0,	1,26
	MS	0,07	0,07	0,05	0,06	0,01	0,05	0,11	0,03	0,05	0,14	0,56	1,27	4,92	2.28	0,19	0,07	0,	0,	9,91
	N	0,07	0,05	0,03	0,01	0,00	0,03	0,06	0,04	0,11	0,35	0,69	0,75	1,60	0.94	0,07	0,06	0,	0,	4,85
	U	0,23	0,15	0,05	0,04	0,02	0,03	0,03	0,04	0,12	0,68	0,80	0,30	0,81	1.44	0,08	0,10	0,	0,	4,92
19-24	VS	0,	0,	0,	0,	0,	0,	0,	0,	0,	0,	0,00	0,	0,03	0.16	0,00	0,	0,	0,	0,20
	MS	0,01	0,02	0,01	0,01	0,	0,00	0,01	0,01	0,02	0,05	0,10	0,12	1,61	1.85	0,02	0,01	0,	0,	3,84
	N	0,03	0,06	0,02	0,01	0,00	0,	0,00	0,01	0,05	0,15	0,35	0,26	1,69	1.54	0,01	0,01	0,	0,	4,18
	U	0,04	0,06	0,01	0,01	0,	0,	0,01	0,01	0,03	0,24	0,35	0,12	0,45	1.21	0,02	0,01	0,	0,	2,60
OVER 24	VS	0,	0,	0,	0,	0,	0,	0,	0,	0,	0,	0,	0,	0,00	0.	0,	0,	0,	0,	0,00
	MS	0,	0,01	0,	0,	0,	0,00	0,	0,00	0,01	0,01	0,01	0,00	0,32	0,63	0,00	0,	0,	0,	0,99
	N	0,00	0,01	0,00	0,	0.	0,	0,01	0,01	0,01	0,06	0,15	0,05	1,19	1.79	0,01	0,	0,	0,	3,28
	U	0,00	0,03	0,01	0,	0,	0,	0,	0,	0,02	0,14	0,20	0,06	0,26	1,02	0,01	0,	0,	0,	1,73
TOTALS	VS	0,03	0,02	0,01	0,02	0,01	0,05	0,05	0,06	0,04	0,10	0,22	0,49	0,79	1,56	0,31	0,07	0,01	0,01	3,86
	MS	0,55	0,53	0,36	0,44	0,49	0,66	0,58	0,42	0,40	0,89	2,02	4,51	10,89	7.06	1,14	0,68	0,14	0,10	31,86
	N	0,87	0,93	0,57	0,68	0,77	0,95	0,54	0,68	0,74	1,60	2,27	2,36	5,86	5,98	1,11	1,10	0,61	0,08	27,71
	U	2,61	2,48	1,21	1,36	1,15	1,45	0,91	1,18	1,45	2,92	2,85	1,71	2,97	6.62	1,92	2,47	1,30	0,03	36,57

TABLE 4. Fall Percentage Frequency Distribution of Wind Speed and Wind Direction at 200-Foot Level vs. Atmospheric Stability

		NNE	NE	ENE	E	ESE	SE	SSE	S	SSW	SW	WSW	W	WNW	NW	NNW	N	VAR	CALM	TOTAL
0 - 3	VS	0,08	0,08	0,06	0,09	0,11	0,19	0,13	0,11	0,08	0,06	0,09	0,14	0,12	0,15	0,17	0,17	0,09	0,20	2,13
	MS	0,42	0,39	0,35	0,40	0,54	0,78	0,36	0,39	0,31	0,35	0,33	0,51	0,57	0,75	0,67	0,65	0,36	1,00	9,13
	N	0,58	0,89	0,59	0,65	0,73	0,65	0,32	0,24	0,19	0,17	0,16	0,25	0,29	0,61	0,77	0,74	0,28	0,68	8,79
	U	0,52	0,56	0,39	0,48	0,31	0,34	0,12	0,09	0,06	0,09	0,07	0,05	0,09	0,19	0,30	0,41	0,23	0,06	4,37
4 - 7	VS	0,05	0,05	0,04	0,04	0,05	0,14	0,17	0,15	0,10	0,13	0,23	0,31	0,31	0,35	0,20	0,09	0,01	0,	2,44
	MS	0,36	0,24	0,20	0,21	0,36	0,67	0,50	0,40	0,42	0,50	0,55	1,11	1,58	1,71	1,11	0,64	0,03	0,	10,58
	N	0,38	0,36	0,25	0,31	0,50	0,51	0,27	0,19	0,20	0,22	0,23	0,27	0,46	1,05	0,81	0,58	0,03	0,	6,61
	U	0,69	0,56	0,36	0,37	0,50	0,46	0,18	0,14	0,18	0,17	0,14	0,13	0,26	0,56	0,85	0,86	0,06	0,	6,48
8 -12	VS	0,01	0,00	0,	0,01	0,	0,04	0,10	0,03	0,02	0,06	0,17	0,40	0,48	0,73	0,20	0,01	0,	0,	2,27
	MS	0,21	0,12	0,07	0,07	0,12	0,34	0,42	0,20	0,24	0,50	0,88	1,66	3,02	2,98	0,93	0,34	0,	0,	12,11
	N	0,17	0,11	0,03	0,04	0,06	0,12	0,13	0,15	0,20	0,35	0,39	0,37	0,55	1,04	0,36	0,18	0,	0,	4,26
	U	0,38	0,21	0,04	0,03	0,04	0,11	0,04	0,05	0,12	0,18	0,22	0,13	0,25	0,79	0,43	0,36	0,00	0,	3,38
13-18	VS	0,00	0,	0,	0,	0,	0,01	0,03	0,00	0,01	0,01	0,05	0,12	0,39	1,02	0,08	0,	0,	0,	1,73
	MS	0,12	0,05	0,01	0,03	0,00	0,12	0,20	0,17	0,20	0,40	0,83	1,04	2,99	2,54	0,25	0,12	0,	0,	9,10
	N	0,13	0,07	0,01	0,01	0,01	0,06	0,07	0,11	0,26	0,58	0,58	0,39	0,70	0,75	0,15	0,11	0,	0,	3,99
	U	0,18	0,09	0,01	0,	0,	0,01	0,03	0,02	0,05	0,20	0,32	0,09	0,33	0,48	0,07	0,12	0,	0,	2,01
19-24	VS	0,	0,	0,	0,	0,	0,	0,00	0,00	0,00	0,00	0,01	0,00	0,05	0,14	0,	0,	0,	0,	0,21
	MS	0,03	0,02	0,02	0,	0,	0,01	0,05	0,13	0,14	0,31	0,39	0,18	0,77	0,79	0,02	0,01	0,	0,	2,86
	N	0,02	0,03	0,01	0,	0,00	0,02	0,03	0,09	0,24	0,56	0,50	0,13	0,43	0,58	0,02	0,02	0,	0,	2,71
	U	0,04	0,03	0,01	0,	0,	0,00	0,01	0,01	0,07	0,22	0,23	0,06	0,19	0,32	0,01	0,02	0,	0,	1,19
OVER 24	VS	0,	0,	0,	0,	0,	0,	0,	0,	0,	0,00	0,	0,	0,	0,	0,	0,	0,	0,	0,00
	MS	0,	0,01	0,	0,	0,	0,	0,02	0,05	0,13	0,14	0,10	0,04	0,13	0,18	0,	0,	0,	0,	0,80
	N	0,01	0,01	0,01	0,	0,	0,	0,01	0,06	0,27	0,58	0,24	0,08	0,26	0,36	0,01	0,00	0,	0,	1,90
	U	0,01	0,04	0,00	0,	0,	0,	0,	0,01	0,08	0,30	0,20	0,05	0,08	0,19	0,01	0,	0,	0,	0,98
TOTALS	VS	0,14	0,14	0,10	0,14	0,16	0,37	0,43	0,30	0,21	0,26	0,56	0,98	1,36	2,39	0,66	0,27	0,10	0,20	8,78
	MS	1,15	0,83	0,65	0,71	1,02	1,92	1,54	1,34	1,45	2,20	3,09	4,53	9,07	8,94	2,97	1,77	0,38	1,00	44,57
	N	1,29	1,48	0,90	1,01	1,29	1,36	0,83	0,85	1,36	2,46	2,10	1,50	2,69	4,38	2,12	1,63	0,31	0,68	28,25
	U	1,83	1,48	0,81	0,88	0,85	0,92	0,37	0,31	0,56	1,16	1,18	0,52	1,19	2,53	1,67	1,77	0,29	0,06	18,41

TABLE 5. Winter Percentage Frequency Distribution of Wind Speed and Wind Direction at 200-Foot Level vs. Atmospheric Stability

		NNE	NE	ENE	E	ESE	SE	SSE	S	SSW	SW	WSW	W	WNW	NW	NNW	N	VAR.	CALM	TOTAL
0 - 3	VS	0.10	0.12	0.07	0.10	0.10	0.22	0.11	0.13	0.11	0.09	0.10	0.14	0.08	0.15	0.19	0.12	0.18	0.12	2.24
	MS	0.49	0.53	0.42	0.54	0.70	1.01	0.67	0.53	0.35	0.38	0.35	0.62	0.62	0.95	0.82	0.88	0.37	1.35	11.57
	N	0.75	0.70	0.61	0.74	0.94	1.00	0.56	0.42	0.28	0.30	0.25	0.50	0.63	0.94	1.08	1.04	0.18	1.92	12.84
	U	0.24	0.24	0.18	0.15	0.17	0.16	0.10	0.04	0.04	0.03	0.02	0.07	0.07	0.11	0.16	0.23	0.05	0.12	2.18
4 - 7	VS	0.10	0.10	0.06	0.08	0.07	0.14	0.12	0.14	0.09	0.12	0.18	0.28	0.22	0.26	0.32	0.19	0.04	0.	2.52
	MS	0.43	0.31	0.27	0.26	0.35	0.57	0.44	0.39	0.31	0.40	0.52	1.00	1.37	2.01	1.60	0.88	0.04	0.	11.15
	N	0.32	0.35	0.25	0.25	0.26	0.34	0.29	0.15	0.12	0.25	0.20	0.42	0.80	1.72	0.91	0.59	0.01	0.	7.22
	U	0.28	0.19	0.12	0.11	0.12	0.12	0.03	0.03	0.04	0.02	0.03	0.05	0.09	0.40	0.38	0.28	0.00	0.	2.31
8 -12	VS	0.01	0.	0.01	0.01	0.01	0.05	0.06	0.05	0.05	0.06	0.11	0.20	0.26	0.61	0.29	0.03	0.	0.	1.82
	MS	0.13	0.09	0.03	0.06	0.10	0.33	0.22	0.15	0.23	0.43	0.81	1.28	2.44	3.92	1.03	0.25	0.00	0.	11.50
	N	0.20	0.09	0.05	0.04	0.08	0.13	0.11	0.08	0.17	0.25	0.23	0.28	1.30	2.61	0.48	0.18	0.	0.	6.28
	U	0.11	0.08	0.03	0.01	0.01	0.03	0.02	0.02	0.06	0.03	0.08	0.04	0.23	0.69	0.19	0.09	0.	0.	1.71
13-18	VS	0.01	0.00	0.	0.	0.	0.01	0.01	0.03	0.02	0.03	0.05	0.12	0.26	0.68	0.08	0.	0.	0.	1.30
	MS	0.10	0.05	0.00	0.01	0.04	0.09	0.16	0.17	0.28	0.68	0.91	1.02	2.16	3.62	0.33	0.08	0.	0.	9.70
	N	0.19	0.05	0.00	0.01	0.02	0.03	0.05	0.14	0.23	0.43	0.43	0.25	0.96	1.61	0.15	0.15	0.	0.	4.71
	U	0.10	0.02	0.01	0.	0.	0.01	0.00	0.01	0.07	0.09	0.14	0.06	0.17	0.31	0.04	0.05	0.	0.	1.09
19-24	VS	0.	0.	0.	0.	0.	0.00	0.01	0.01	0.01	0.01	0.01	0.02	0.03	0.05	0.00	0.	0.	0.	0.15
	MS	0.01	0.02	0.	0.	0.00	0.03	0.07	0.12	0.24	0.67	0.45	0.28	0.44	0.71	0.03	0.01	0.	0.	3.08
	N	0.05	0.03	0.	0.00	0.01	0.01	0.04	0.10	0.25	0.54	0.31	0.14	0.14	0.25	0.03	0.08	0.	0.	1.99
	U	0.04	0.03	0.01	0.	0.	0.00	0.00	0.02	0.03	0.09	0.10	0.01	0.05	0.12	0.00	0.03	0.	0.	0.54
OVER 24	VS	0.	0.	0.	0.	0.	0.00	0.	0.01	0.01	0.01	0.	0.00	0.	0.	0.	0.	0.	0.	0.02
	MS	0.01	0.00	0.	0.	0.	0.01	0.05	0.13	0.38	0.53	0.27	0.08	0.09	0.09	0.00	0.00	0.	0.	1.64
	N	0.05	0.02	0.	0.	0.	0.01	0.01	0.11	0.50	0.73	0.25	0.07	0.05	0.06	0.01	0.05	0.	0.	1.91
	U	0.03	0.01	0.	0.	0.	0.	0.00	0.01	0.06	0.19	0.13	0.02	0.01	0.04	0.00	0.01	0.	0.	0.51
TOTALS	VS	0.22	0.23	0.14	0.19	0.18	0.43	0.32	0.35	0.29	0.32	0.45	0.76	0.85	1.76	0.88	0.35	0.22	0.12	8.07
	MS	1.18	1.00	0.72	0.87	1.20	2.04	1.61	1.48	1.80	3.07	3.31	4.28	7.11	11.30	3.81	2.10	0.41	1.35	48.64
	N	1.58	1.25	0.91	1.04	1.30	1.51	1.06	1.00	1.56	2.48	1.67	1.66	3.87	7.19	2.66	2.09	0.19	1.92	34.95
	U	0.78	0.57	0.35	0.26	0.30	0.32	0.16	0.13	0.29	0.46	0.50	0.25	0.61	1.67	0.78	0.70	0.05	0.12	8.34

Selection of angular width for the sector-averaged plume is governed by the form of available wind direction data. Table 2 shows that Hanford wind data have been compiled in 16 direction sectors. As a result, the plume width has been set at 22.5° for this study. The mixing height tends to vary diurnally and seasonally with the greatest heights generally found on summer afternoons and the lowest on winter nights. We will ignore the known diurnal variation and assume a constant mixing height for each season, as shown in Table 6. A recent series of measurements at Hanford is expected to provide better information on mixing heights.

TABLE 6. Assumed Heights of the Mixed Layer by Season

Season	Height
Spring	1000 m
Summer	1500 m
Fall	1000 m
Winter	500 m

Hanford Sky Cover Climatology

Sky cover is observed and recorded each hour at the Hanford Meteorology Station. At the end of each month, the average sky cover for daylight hours is computed and published internally for use by the Hanford contractors. The sky cover data in Reference 28, in these monthly summaries, and in a random sample of data taken from the original records form the basis of the climatology presented here.

Annual and monthly sky cover averages for Hanford are presented in Table 7 for several different data sets. It should be noted that for every month the sky cover during daylight hours is equal to or greater than the 24 hour average.

This is an indication that convective activity, caused by solar heating, is a significant factor in the cloud formation processes at Hanford.

The last column in Table 7 gives the standard deviation of the monthly sky cover averages for the period 1967 through 1977. They are negatively correlated with the mean sky cover. That is, high average sky covers are associated with small standard deviations. This means that the year to year variability in sky cover in the winter is less than that for the summer. As a result a given change in the long term average sky cover would be easier to detect statistically in the winter than it would be in the summer.

TABLE 7. Monthly and Annual Sky Cover (in Tenths) for Hanford with Standard Deviation of Monthly Averages of Sky Cover for Daylight Hours about the Mean for the Period 1967-1977

	All Hours 1967-1970	Daylight 1946-1975	Daylight 1967-1977	St. Dev. 1967-1977
January	7.6	7.8	8.0	.58
February	6.9	7.4	7.4	.74
March	6.2	6.8	7.0	.67
April	6.1	6.4	6.6	.68
May	5.5	5.8	6.0	.72
June	4.9	5.3	5.4	.96
July	2.7	2.8	3.3	1.02
August	3.1	3.2	3.2	1.54
September	4.0	4.0	4.0	1.41
October	5.5	5.9	6.0	1.13
November	7.0	7.6	8.0	.77
December	7.8	8.1	8.0	.58
Annual Average	5.6	5.9	6.1	

Average sky cover is given in Table 8 for each hour for the mid-day period between 0800 and 1600 PST by months. During the months of November through February the sky cover is a maximum in the morning about sunrise. During the remainder of the year it is a maximum in the mid to late afternoon. The diurnal variation in sky cover is less than 2 tenths in all months and is greatest in the spring and fall. The diurnal variation is relatively small compared with the annual variation of monthly averages.

TABLE 8. Mid-Day Variation of Monthly Average Sky Cover (in tenths)

	TIME (PST)								
	8	9	10	11	12	13	14	15	16
January	8.3	8.2	8.2	8.1	8.1	8.1	8.0	8.0	8.1
February	7.6	7.6	7.5	7.3	7.4	7.4	7.4	7.4	7.4
March	6.8	6.7	6.6	6.8	6.9	7.0	7.0	6.9	6.9
April	6.3	6.3	6.4	6.5	6.7	7.0	7.0	6.9	7.0
May	5.4	5.5	5.6	5.8	6.0	6.2	6.1	6.3	6.4
June	4.7	4.8	5.0	5.3	5.2	5.3	5.3	5.4	5.6
July	2.5	2.4	2.5	2.6	2.8	2.9	3.0	3.1	3.2
August	3.2	3.0	3.2	3.2	3.3	3.4	3.5	3.6	3.7
September	4.3	4.2	4.3	4.3	4.3	4.4	4.4	4.4	4.4
October	5.8	5.8	5.8	5.8	6.0	6.2	6.3	6.4	6.4
November	7.7	7.6	7.4	7.4	7.6	7.7	7.6	7.5	7.3
December	8.4	8.3	8.5	8.4	8.3	8.2	8.1	8.1	8.0

Hanford Solar Radiation Climatology

Solar radiation is measured at the Hanford Meteorological Station using a calibrated Eppley Pyranometer. Signals from the device are continuously recorded on a strip chart and reduced manually to determine the solar radiation received each hour.

The average daily solar radiation at Hanford is given in Table 9 by month for the periods 1953 through 1975 and 1967 through 1977. The standard deviations of the individual monthly averages in the 1967-1977 period are given in the third column. The final two columns of the table involve the solar radiation received at the top of atmosphere above Hanford. The incident radiation estimates in column 4 are taken from Reference (29). The last columns shows that the fraction of the incident radiation received at the surface varies from about 40% in the winter to slightly over 70% in July. One of the major factors affecting this fraction is sky cover.

Diurnal variation of the monthly average solar radiation between 0800 and 1600 PST is shown in Table 10. The maximum insolation occurs in July for the hour beginning at 1100 PST, rather than in June. Again this can be attributed to the difference in cloudiness between July and July.

SPECIFIC HNEC SKY COVER AND SOLAR RADIATION MODELS

The final topic to be covered prior to the presentation of the study results is the development of HNEC specific models for the conversion of cooling system effluent concentrations to changes in sky cover and solar radiation. In this section we will deal with the change in sky cover first and then the change in solar radiation. We will end the section with a quick check on the consistency of our models with existing information.

TABLE 9. Average Daily Solar Radiation (ly day^{-1})

	Daily Total 1953-1975	Daily Total 1967-1977	Standard Deviation 1967-1977	Incident at Top of Atmosphere	Fraction Received at Sfc
January	120	118	14	260	.46
February	202	203	11	400	.50
March	340	338	22	580	.59
April	475	472	43	780	.61
May	576	584	30	910	.63
June	628	630	31	950	.66
July	659	650	42	920	.72
August	558	556	49	830	.67
September	423	415	38	650	.65
October	262	268	24	450	.58
November	132	130	17	300	.44
December	92	93	18	220	.42
Annual	372	372		605	.61

TABLE 10. Mean Solar Radiation (ly hr^{-1}) by Month and Hour

	TIME (PST)								
	08	09	10	11	12	13	14	15	16
January	4.8	11.7	17.3	21.4	21.9	18.8	13.6	6.8	1.3
February	11.1	19.8	27.8	32.4	33.1	30.0	24.1	15.6	6.0
March	24.0	35.3	43.6	48.7	48.2	43.9	36.9	26.4	14.6
April	38.6	49.4	56.7	58.7	57.7	52.0	45.1	34.1	22.1
May	47.8	58.0	64.2	67.2	63.7	59.7	52.8	42.1	29.4
June	52.1	61.4	67.6	70.5	69.2	63.8	56.3	46.2	34.1
July	53.1	63.5	71.1	74.7	73.8	69.0	61.7	50.7	37.6
August	44.6	55.5	63.0	66.0	66.1	62.7	53.5	42.2	29.0
September	34.8	45.7	53.4	56.0	55.6	50.3	40.9	29.4	16.4
October	22.2	31.6	38.3	41.2	39.8	33.8	24.9	14.8	5.0
November	9.8	17.0	22.0	24.0	23.0	18.9	13.0	5.6	0.6
December	4.2	9.7	14.5	17.3	17.3	14.5	9.2	3.4	0.1

Sky Cover Increase

The conversion factor that relates changes in sky cover to cooling system effluent concentration will be assumed. However, prior to stating the assumption, we will examine additional information that should be related to the conversion.

Figure 3 shows the diurnal variations of sky cover and temperature and relative humidity near ground level for January, April, July and October. In the winter the diurnal sky cover variation is small, the temperatures are generally low and the relative humidity is high. Under these conditions we will assume that cooling system effluents might cause an increase in cloudiness due to triggering convective activity or they might simply saturate the air. In the former event only a portion of the available clear sky would be covered by an increase in

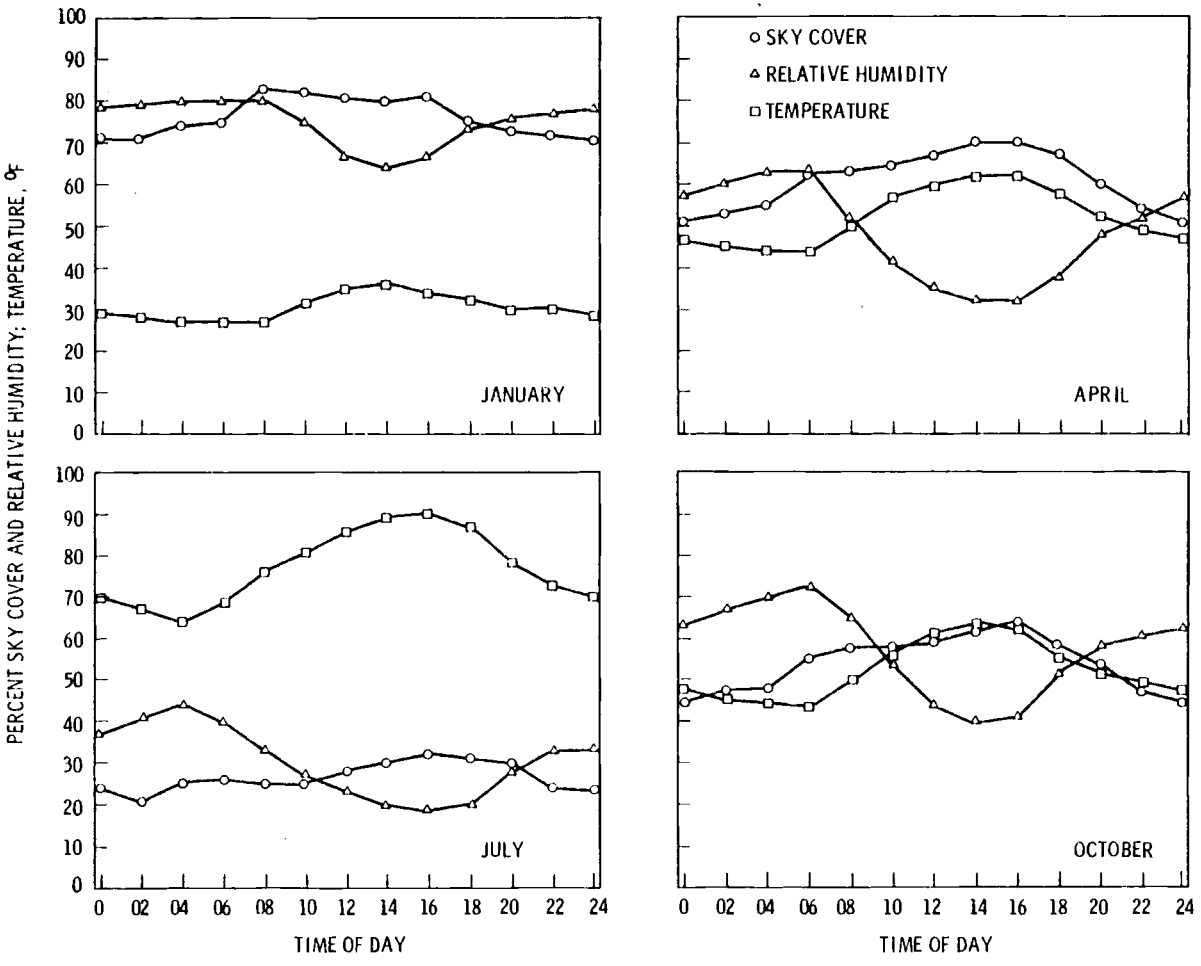

FIGURE 3. Diurnal Variation of Sky Cover, Relative Humidity and Temperature for January, April, July and October

cloudiness and in the latter all the clear sky would be covered.

In the remaining seasons the temperatures are sufficiently high that the probability of saturating a large volume of air is remote. As a result increases in cloudiness would be associated with increased convective activity. The large diurnal variation in sky cover shown for the spring and fall indicates that the atmosphere is generally ready for the formation of clouds if convective activity can be initiated. The diurnal variation in sky cover is relatively small in the summer, even though the temperature variation is high. This indicates that convective activity, although associated with the production of clouds, is not as efficient as it is in the spring and fall. As a result, in our conversion from effluent concentration to sky cover increase a given effluent concentration will be assumed to cause a larger fractional increase in sky cover in the spring and fall than it does in the summer. During these seasons, the maximum fractional increase in sky cover will be less than 100% of the available free sky.

Having established this background, we assume the conversion factors presented in Table 11. Earlier we assumed that water concentration would be a tracer for the cooling system effluents, thus Table 11 uses increased water content as the independent variable.

The actual conversion between effluent concentration and increased sky cover is unknown, therefore this table represents a significant weakness in the study. However, the conversions assumed probably will result in over estimation of the increase in sky cover. To ensure that a maximum increase in cloudiness is evaluated, we will run each of the mid season months with a worst case conversion table. In that table an increase of water content of 0.1 g m^{-3} will result in a 100% fractional increase in cloudiness, i.e., the sky cover will increase to 10/10.

TABLE 11. Conversion Table Relating an Increase in Water Content to an Increase in Sky Cover

Winter		Spring		Summer		Fall	
$\Delta\rho_v$ ($g\ m^{-3}$)	f_i	$\Delta\rho_v$ ($g\ m^{-3}$)	f_i	$\Delta\rho_v$ ($g\ m^{-3}$)	f_i	$\Delta\rho_v$ ($g\ m^{-3}$)	f_i
< 0.1	0	< .25	0	< .25	0	< .25	0
0.1 to 0.3	.2	.25 to .50	.2	.25 to .50	0.1	.25 to .50	.2
0.3 to 0.5	.5	.50 to 1.0	.4	.50 to 1.0	0.3	.50 to 1.0	.4
> 0.5	1.0	> 1.0	.8	> 1.0	0.5	> 1.0	.8

The Relationship Between Sky Cover and Solar Radiation

Intuition leads us to expect an inverse relationship between sky cover and solar radiation. This expectation is borne out by data as is shown in Figure 4, which shows the annual variation of monthly averages. It is particularly evident in the increase in insolation between June and July although Table 9 shows that the solar radiation received at the top of the atmosphere decreases.

For current purposes, it is necessary to relate hourly rather than monthly averages. Some guidance is provided in Reference (19) through (23) which treat this relationship on a month by month basis. To develop a single relationship that can be used for all months, we will normalize observed solar radiation to the long-term mean for the month and time of day of the observation and relate sky cover observations to an appropriate mean. Normalized solar radiation is simply $SR/\overline{SR}$, but the normalized sky cover expression is more complex. To obtain a nondimensional sky cover variable with a range of zero to two, and a value of one when the sky cover is equal to the mean value, we make the following transformation:

$$\xi = \begin{cases} \dfrac{SC}{\overline{SC}} & SC \leq \overline{SC} \qquad (11a) \\ 1 + \dfrac{SC - \overline{SC}}{10 - \overline{SC}} & SC \geq \overline{SC} \qquad (11b) \end{cases}$$

where ξ is the nondimensional sky cover.

Initially we will treat the case of low level clouds (ceiling below 10,000'). Then we will treat the case of high level clouds.

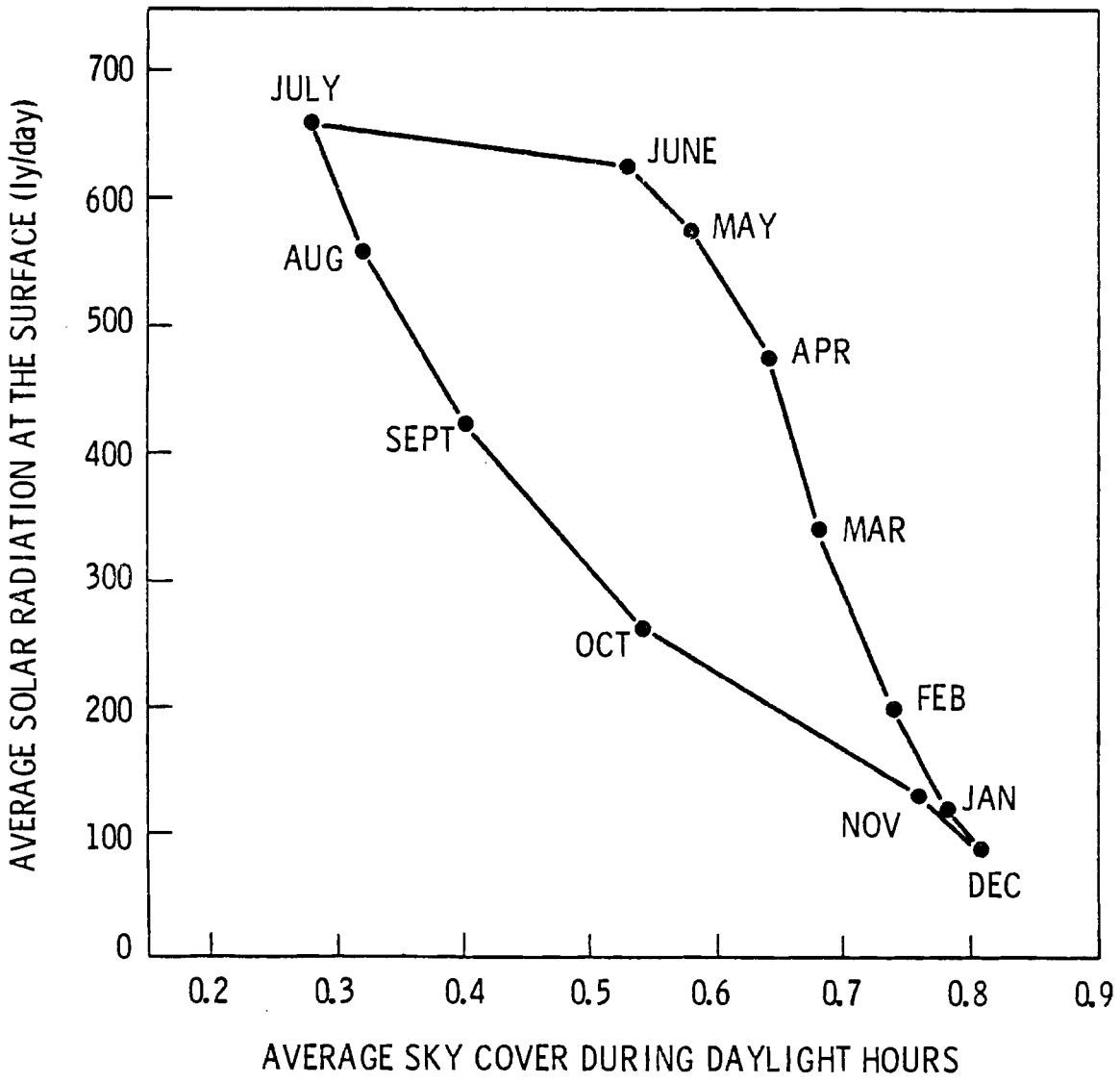

FIGURE 4. Annual Variation of Average Sky Cover and Solar Radiation

Matveev[19] cites a number of studies in this area and gives linear, quadratic and exponential models for the sky-cover insolation relationship. Other authors[20-23] tend to favor a quadratic model, although the model forms are not completely comparable. As a result, for the low cloud case we will try three models and compare the results. The models are:

$$1.\quad F(SC^*,\overline{SC}) = G_1(\xi) = a_o + a_1\xi \quad , \tag{12a}$$

$$2.\quad F(SC^*,\overline{SC}) = G_2(\xi) = b_o + b_1\xi + b_2\xi^2 \quad , \tag{12b}$$

and

$$3.\quad F(SC^*,\overline{SC}) = G_3(\xi) = c_o\exp(c_1\xi^{c2}) \tag{12c}$$

The constants in these models can be evaluated using the random data sample taken from the period 1967 through 1977. Average values of normalized solar radiation were computed for $\xi = 0$ and $\xi = 2$ using the 0900, 1200 and 1500 observations. These averages are given in Table 12 along with the standard errors in the estimates of the averages. Constants in G_1 were evaluated using these values. The constants in G_2 and G_3 were evaluated using these values along with the assumption that $SR/\overline{SR} = 1$ when $\xi = 1$. Model constants are given in Table 13, and the three models are compared with a small data sample in Figure 5.

The literature (e.g., References (24), (26) and (27)) indicates that high clouds, particularly cirriform clouds, have relatively little effect on insolation. Table 12 shows that for Hanford, when $\xi = 2$ and the ceiling is above 10,000 ft, the average normalized solar radiation is 1.10. As a result, we will assume that $F(SC,\overline{SC})$ is 1.10 for all values of ξ if there is a high ceiling. Figure 6 shows data for high clouds and the line representing $SR/\overline{SR} = 1.10$.

TABLE 12. Average and Standard Error of Normalized Solar Radiation During Clear and Overcast Skies at Hanford

ξ	$\overline{(SR/\overline{SR})}$	Standard Error
0	1.25	.05
2 (low ceilings)	.56	.08
2 (high ceilings)	1.10	.07

TABLE 13. Coefficient Values for the Models Relating Changes in Sky Cover and Solar Radiation

Model		i		
		0	1	2
1	a_i =	1.25	-.345	
2	b_i =	1.25	-.155	- .095
3	c_i =	1.25	-.223	+1.85

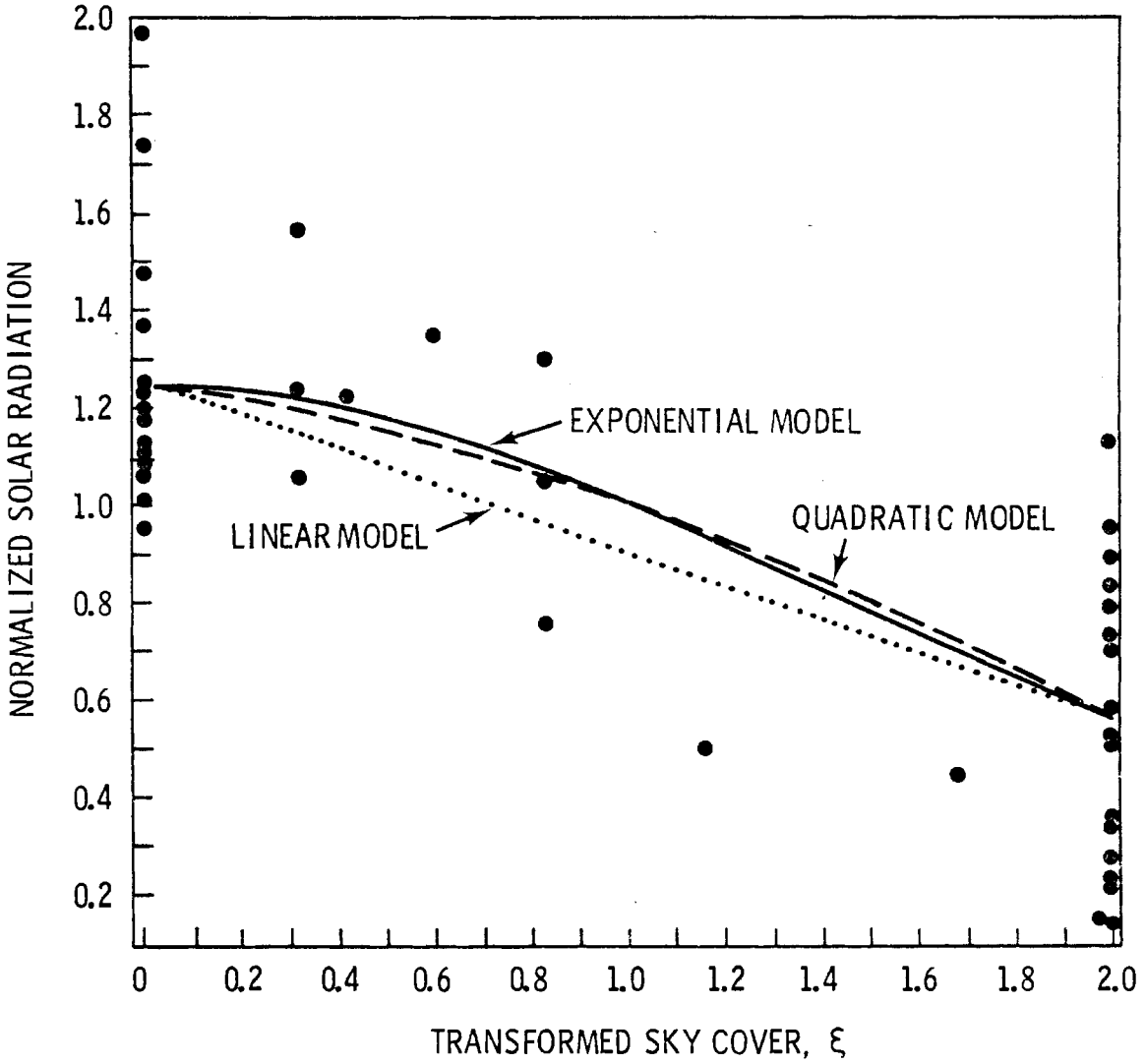

FIGURE 5. The Relationship Between Normalized Solar Radiation and Transformed Sky Cover for Low Clouds.

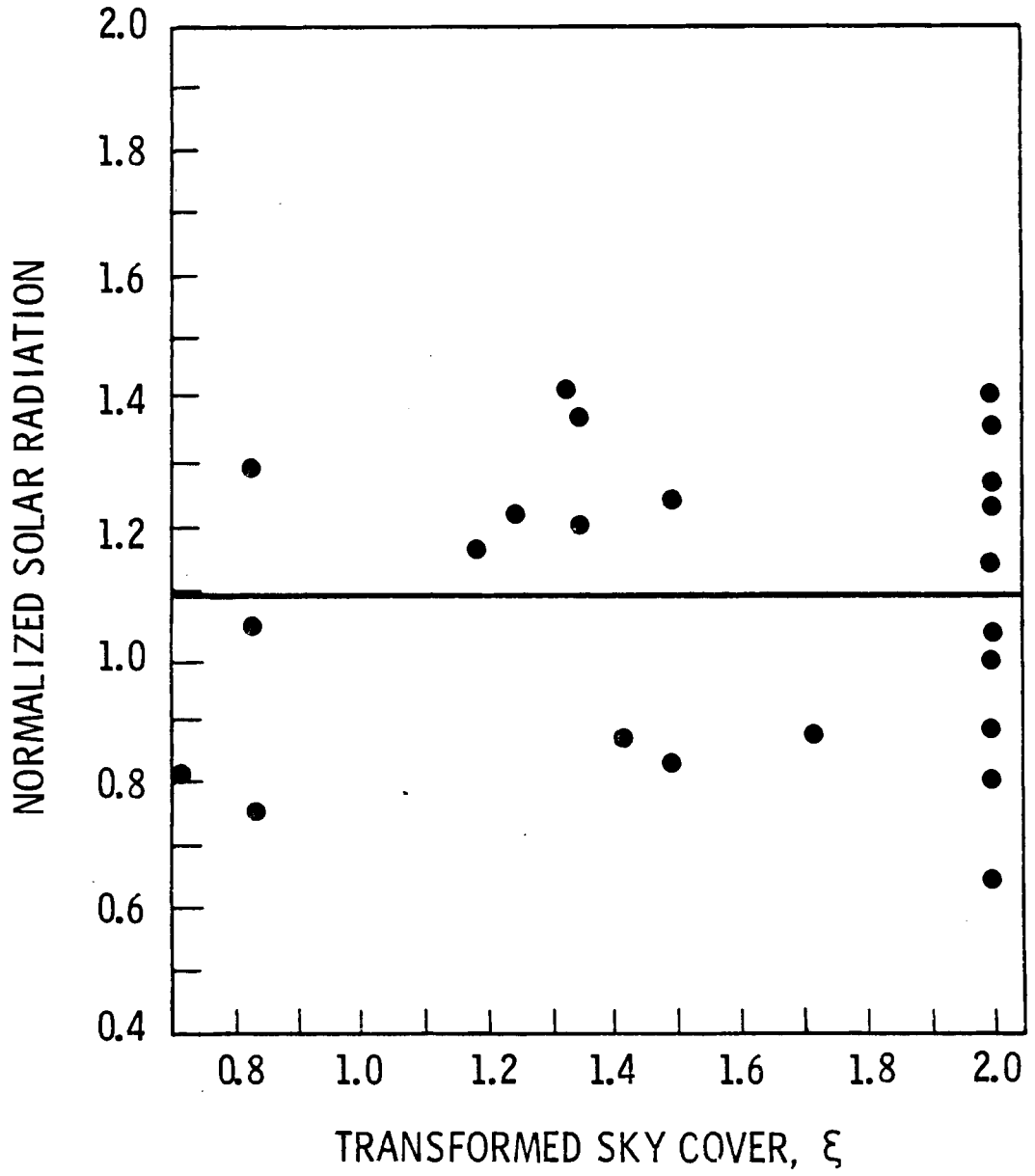

FIGURE 6. The Relationship Between Normalized Solar Radiation and Transformed Sky Cover for High Clouds

Both Figures 5 and 6 show a significant amount of scatter in the data. This is to be expected because we have not accounted for position of the clouds relative to a direct line between the sun and the pyreheliometer. Other factors contributing to the scatter include cloud type and atmospheric turbidity.

Consistency of the HNEC Specific Models

In developing the sky cover and solar radiation models in the preceeding chapter we indicated a need for the sky cover frequency distributions for each month. The distributions assumed are presented in Table 14. Although the distributions are assumed, they are based on the information contained in Table 23 of Reference 28 and have been adjusted to give appropriate mean sky covers. The division of sky cover between high and low ceiling categories was adjusted using solar radiation data and the random data sample.

When we substitute these frequency distributions into Equation (10), we get:

$$\frac{\overline{SR}}{\overline{SR}_o} = \sum_{SC^*} F(SC,\overline{SC})\,P(SC) \quad . \tag{13}$$

If the solar radiation model $F(SC,\overline{SC})$ and the frequency distribution $P(SC)$ are both correct then $\overline{SR}$ will be equal to $\overline{SR}_o$ and the summation will equal 1.

Table 15 presents a comparison of the average sky cover computed from the assumed frequency distributions with climatological values and the values of the summation in Equation (13). The summations were carried out for mid-season months for the linear and quadratic models for $F(SC,\overline{SC})$, and for all months for the exponential model. In each case, the

TABLE 14. Assumed Initial Sky Cover Frequency Distributions

Sky Cover (tenths)	Jan	Feb	Mar	Apr	May	Jun	Jul	Aug	Sep	Oct	Nov	Dec
0	.04	.08	.10	.08	.12	.15	.40	.36	.34	.17	.06	.03
1	.02	.04	.05	.04	.05	.06	.10	.10	.08	.06	.04	.03
2	.02	.03	.04	.04	.05	.06	.08	.08	.05	.05	.03	.03
3	.02	.03	.04	.04	.05	.06	.07	.07	.04	.04	.03	.03
4	.03	.03	.04	.05	.07	.06	.06	.07	.04	.04	.03	.03
5	.03	.03	.04	.05	.08	.06	.04	.06	.04	.04	.03	.03
6	.03	.03	.04	.06	.04	.06	.04	.05	.04	.04	.03	.03
7	.04	.03	.04	.06	.06	.05	.04	.03	.04	.04	.03	.03
8	.07	.03	.03	.08	.07	.05	.01	.01	.03	.04	.04	.03
9	.10	.08	.03	.08	.07	.06	.01	.01	.04	.04	.04	.04
10	.15	.20	.15	.09	.07	.07	.11	.11	.10	.15	.20	.23
6*	.03	.03	.04	.05	.04	.05	.01	.01	.03	.03	.03	.02
7*	.03	.03	.04	.06	.05	.05	.01	.01	.03	.04	.03	.02
8*	.08	.03	.03	.07	.06	.05	.01	.01	.03	.03	.04	.03
9*	.12	.06	.04	.07	.06	.05	.01	.01	.03	.04	.05	.06
10*	.19	.24	.25	.08	.06	.06	.01	.01	.04	.15	.30	.33

*Ceiling above 10,000 ft

TABLE 15. Check on the Internal Consistency of Assumed Monthly Sky Cover Distributions and the Sky Cover Insolation Models

	Average Sky Cover		Normalized Solar Radiation		
			Model		
	Actual Daylight Hours	Assumed PDF	Linear	Quadratic	Exponential
January	7.8	7.8	.96	.99	.99
February	7.4	7.4			.98
March	6.8	6.8			1.02
April	6.4	6.4	.97	1.01	1.01
May	5.8	5.7			1.02
June	5.3	5.4			1.03
July	2.8	3.1	1.03	1.07	1.07
August	3.2	3.2			1.02
September	4.0	4.1			1.05
October	5.9	5.9	.99	1.02	1.02
November	7.6	7.7			1.00
December	8.1	8.1			.98

assumed distribution appears to be reasonable. However, the data in Table 15 are only an indication of reasonableness. They do not prove that the distributions are correct. At best the data show that sky cover distributions and solar radiation models are internally consistent with readily available climatological data.

RESULTS

The development of the analytical tools for estimating changes in sky cover and solar radiation for the current study has been completed. It is clear that they are rudimentary. They are, in fact, a collection of "back of the envelope models" that only provide an indication of the order of magnitude of the potential changes. As we examine the results presented here, we must continually remember that the precision in the numerical values is not an indication of the precision of the estimates.

Predicted increases in sky cover are given in Table 16 for 6 areas in and around the HNEC. Each estimate is a spatial average. The HNEC estimates are averages for the area in the immediate vicinity of the assumed cluster locations. The Tri-Cities estimates are averages for the entire Richland, Kennewick, Pasco area. The ALE estimates are for the Arid Land Ecology study area along the southwest border of the Hanford Area. Wahluke Slope borders the northern side of the Hanford, and the Mesa-Eltopia area lies directly east of Hanford. Finally the Yakima Valley estimates are for the area around Sunnyside, Grandview and Prosser.

Examining Table 16 we see the expected result that the maximum increases in sky cover occur in the immediate vicinity of the HNEC clusters. The predicted increases in average sky cover for the spring, fall and winter are statistically significant assuming an observation period of 11 years following completion of the HNEC and an unchanged sky cover variance. The predicted increases during the summer are not statistically significant.

Off the Hanford Area the greatest changes in sky cover are predicted for the Mesa-Eltopia and Tri-Cities areas. However, These increases are not statistically significant.

TABLE 16. Predicted Increase in Sky Cover (in tenths)

	Existing $\overline{SC}$ Daylight Hours (tenths)	HNEC	Tri-Cities	ALE	Wahluke Slope	Mesa/Eltopia	Yakima Valley
January	7.8	1.0**	0.3	0.2	0.2	0.4	0.1
February	7.4	1.2**	0.4	0.2	0.2	0.4	0.2
March	6.8	0.7*	0.1	0.1	0.1	0.3	0.1
April	6.4	0.8**	0.1	0.1	0.1	0.3	0.1
May	5.8	0.9**	0.2	0.1	0.1	0.4	0.1
June	5.3	0.4	0.1	0.1	0.1	0.1	<
July	2.8	0.6	0.1	0.1	0.1	0.2	0.1
August	3.2	0.6	0.1	0.1	0.1	0.2	<
September	4.0	1.6**	0.4	0.3	0.3	0.6	0.2
October	5.9	1.1*	0.3	0.2	0.2	0.4	0.1
November	7.6	0.6*	0.2	0.2	0.1	0.2	0.1
December	8.1	0.9**	0.3	0.2	0.1	0.3	0.1

*Significant at the 95% confidence level
**Significant at the 99% confidence level

< less than .05

At this point we should briefly discuss statistical significance. In testing statistical significance we use Student's t test between means[30], and assume that we have no more information about either sky cover or solar radiation than provided by records of routine observations. We do not consider a predicted change significant unless we have at least 95% confidence that the difference between the current climatological mean and the predicted mean would not result from normal variation between data samples. The fact that a change is evaluated as not statistically significant does not mean it wouldn't occur, only that it would be difficult to detect within the time specified because of normal variability of the atmosphere.

During the course of the study complete sets of computations were made using different initial sky cover distributions. The computations indicate that the predicted changes in sky cover and solar radiation are not particularly sensitive to moderate changes in the assumed sky cover distributions if the mean sky cover remains relatively constant. However the results are rather sensitive to changes in the mean sky cover.

Increases in sky cover would be aesthetically displeasing, however that would be difficult to evaluate. They would also result in decreases in solar radiation. Tables 17 and 18 present the changes in solar radiation that are predicted to result from an operating HNEC.

Table 17 compares decreases in solar radiation predicted by the three models relating changes in sky cover to changes in insolation. Perusal of the table rapidly leads to the conclusion that the predicted decrease is not particularly sensitive to the model used within the limits of those tested. Throughout the remainder of this report, the estimated changes in insolation are results obtained using the exponential model.

TABLE 17. Comparison of the Results from Linear, Quadratic and Exponential Models for the Relationship Between Sky Cover and Solar Radiation. Tabled Values are Predicted Decreases in Insolation (ly/day)

	Model	HNEC	Tri-Cities	ALE	Wahluke Slope	Mesa/Eltopia	Lower Yakima Valley
January	linear	23	8	5	4	10	3
	quadratic	24	8	5	4	10	3
	exponential	24	9	5	4	10	3
April	linear	53	10	7	7	18	4
	quadratic	49	9	6	6	20	4
	exponential	51	9	6	6	21	4
July	linear	39	6	5	5	13	3
	quadratic	31	4	4	4	11	2
	exponential	32	5	4	4	11	2
October	linear	35	9	6	6	14	4
	quadratic	33	8	6	5	12	4
	exponential	33	9	6	6	11	4

The greatest impact on solar radiation is seen in Table 18 to be in the immediate vicinity of the clusters. In general, the predicted reductions in solar radiation are about 20% in the winter, 10 to 15% in the spring and fall, and 5% in the summer. Except for August, the decreases are statistically significant. In most cases, we would have 99% confidence that the predicted decreases was not a normal variation.

The offsite impacts are greatest in the Mesa-Eltopia and Tri-Cities areas as expected from the changes in sky cover. But, we note that the decreases in solar radiation predicted for these areas for February and for the Mesa-Eltopia area for March and May are statistically significant even though the changes in sky cover were not significant. We further note that each significant change in sky cover is paired with a significant decrease in solar radiation. This leads to the conclusion that changes in solar radiation would be a more sensitive indicator of an atmospheric modification than changes in sky cover. This conclusion is reasonable and might have been expected since insolation measurements are much more precise than sky cover estimates. It might also have been expected because the coefficient of variance of the monthly average insolation is significantly smaller than that for monthly average sky cover.

The combined effects of the sky cover and solar radiation changes for the area in the vicinity of the HNEC clusters are summarized in Figure 7. The current relationship, shown in Figure 4, is shown in dashed lines for comparison. The obvious change to be noted is the shift of the enclosed area toward increased cloudiness and lower insolation. There is also a change in the shape of the area, which indicates a more rapid or earlier shift from summer to fall and more gradual but delayed shift from spring into summer. The ecological significance of these changes needs evaluation.

TABLE 18. Predicted Decrease in Solar Radiation (ly/day)

	Existing $\overline{SR}$ (ly/day)	HNEC	Tri-Cities	ALE	Wahluke Slope	Mesa/Eltopia	Yakima Valley
January	120	24 **	9	5	4	10	3
February	202	40 **	14 **	8	7	16 **	5
March	340	40 **	7	5	5	17 *	3
April	475	51 **	9	6	6	21	4
May	576	62 **	11	8	8	25 *	5
June	628	36 **	5	4	4	12	2
July	659	32 *	5	4	4	11	2
August	558	26	4	3	3	9	2
September	423	56 **	14	10	9	20	7
October	262	34 **	9	6	6	11	4
November	132	15 **	5	3	3	6	2
December	92	18 *	7	4	3	8	2

*Significant at the 95% confidence level
**Significant at the 99% confidence level

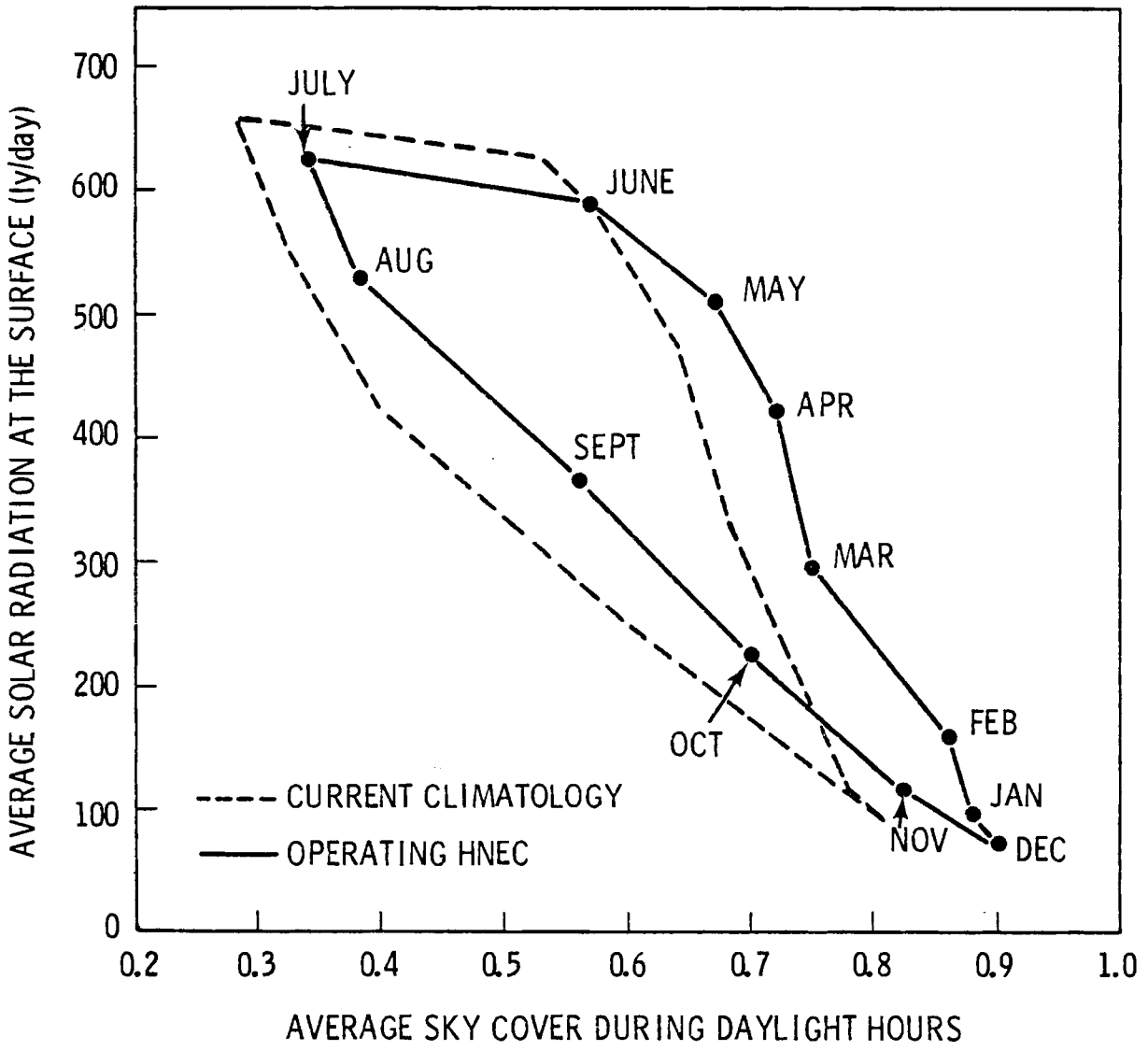

FIGURE 7. The Predicted Variation of Average Sky Cover and Solar Radiation in the Vicinity of an Operating HNEC

Earlier we discussed the uncertainty in the conversion from cooling system effluent concentration to increase in sky cover, and promised to compare the estimated changes with "worst case" estimates. Those comparisons are presented in Tables 19 and 20.

In general, the "worst case" changes in sky cover and solar radiation for January are only slightly larger than those estimated originally. In April and October the worst cases changes are about a factor of two larger than those originally estimates, and in July the "worst case" estimates are larger by a factor of 4 or more.

In the Mesa-Eltopia Area the "worst case" changes in both sky cover and solar radiation are statistically significant for each month for which they were evaluated. In the Tri-Cities, the worst case sky cover increases are statistically significant for January as are the solar radiation decreases for January and October. In the other areas even the "worst case" changes are not considered statistically significant.

TABLE 19. Comparison of Predicted Increases in Sky Cover with Worst Case Values

		January	April	July	October
HNEC	P	1.0**	.8**	.6**	1.1**
	WC	1.0**	1.6**	3.4**	7.9**
Tri-Cities	P	.3	.1	.1	.3
	WC	.4	.4	.6	.6
ALE	P	.2	.1	.1	.2
	WC	.2	.2	.4	.4
Wahluke Slope	P	.2	.1	.1	.2
	WC	.2	.2	.3	.3
Mesa/Eltopia	P	.4	.3	.2	.4
	WC	.6*	1.0**	1.6**	1.0*
Yakima Valley	P	.1	.1	.1	.1
	WC	.1	.1	.2	.2
Existing Mean Sky Cover (daylight hours)		7.8	6.4	2.8	5.9

*Significant at the 95% confidence level
**Significant at the 99% confidence level

TABLE 20. Comparison of Predicted Decreases in Solar Radiation with Worst Case Values

		January	April	July	October
HNEC	P	24**	51**	32**	34**
	WC	25**	95**	151**	54**
Tri-Cities	P	9	9	5	9
	WC	11*	23	24	19*
ALE	P	5	6	4	6
	WC	5	13	15	10
Wahluke Slope	P	4	6	4	6
	WC	5	13	14	10
Mesa/Eltopia	P	10	21	11	11
	WC	13*	57**	72**	30**
Yakima Valley	P	3	4	2	4
	WC	3	8	10	7
Existing Mean Solar Radiation (ly/day)		120	475	659	262

*Significant at the 95% confidence level
**Significant at the 99% confidence level

CONCLUSIONS

Using a combination of "back of the envelope" models we have estimated the changes in sky cover and solar radiation that might result from the operation of a Hanford Nuclear Energy Center. We have assumed that the center is composed of 20 power reactors using mechanical draft cooling towers and that all reactors operate continuously. In addition, we have assumed that the climatological conditions of the Hanford Meteorological Station are representative of the current conditions for the entire area surrounding the HNEC. Again we must remember that the models used are rudimentary and that numerical precision does not indicate model accuracy.

Based on the models and these assumptions we have arrived at the following conclusions:

1) Increases in sky cover and decreases in solar radiation resulting from the operation of an HNEC would generally be small outside the immediate vicinity of the reactor clusters.

2) The changes in sky cover and solar radiation in the immediate vicinity of the clusters would be statistically significant during the fall, winter and spring. During the summer, the decreases in June and July solar radiation would also be significant.

3) The decreases in solar radiation predicted for the Mesa-Eltopia area for February, March and May are statistically significant, as is the decrease in the Tri-Cities for February.

4) When "worst case" assumptions are made for the conversion of cooling system effluent concentrations to increases in sky cover, the estimated changes in both

sky cover and solar radiation from the original estimates range from a few percent in January to a factor of 4 or more in July.

5) The predicted changes in sky cover and solar radiation are not particularly sensitive to changes in the initial sky cover distribution if the mean sky cover remains reasonably constant, and the changes in solar radiation are not sensitive to the model relating sky cover and insolation.

6) Changes in solar radiation are likely to be a more sensitive indicator of atmospheric modification than are changes in sky cover.

In addition, it is readily apparent that the wind direction distribution is one of the most important factors considered. The specific impacts predicted at a given receptor depend to a large extent on the position of the receptor relative to the HNEC and on the wind direction distribution.

The predicted changes in sky cover and solar radiation have been evaluated for statistical significance, which relates to our ability to detect the change. Further studies are needed to evaluate the social and ecological significance of the predicted changes.

REFERENCES

1. The Hanford Nuclear Energy Center A Preliminary Conceptual Study, BNWL-B-332, Battelle, Pacific Northwest Laboratories, Richland, WA, January 1974, 316 p.

2. The Hanford Nuclear Energy Center An Interim Conceptual Study, BNWL-B-458, Battelle, Pacific Northwest Laboratories, Richland, WA, October 1975, 66 p.

3. The Hanford Nuclear Energy Center An Interim Conceptual Study, BNWL-B-458 II, Battelle, Pacific Northwest Laboratories, Richland, WA, Nobember 1976, 51 p.

4. Electric Power Transmission for a Hanford Nuclear Energy Center, BNWL-B-426, Battelle, Pacific Northwest Laboratories, Richland, WA, September 1975, 69 p.

5. Status Report - Conceptual Fuel Cycle Studies for the Hanford Nuclear Energy Center, BNWL-B-437, Battelle, Pacific Northwest Laboratories, Richland, WA, November 1975, 41 p.

6. Heat Sink Management for a Hanford Nuclear Energy Center, BNWL-B-448, Battelle, Pacific Northwest Laboratories, Richland, WA, November 1975, 51 p.

7. Young, J. R., L. D. Kannberg, J. V. Ramsdell, W. H Richard and D. G. Watson, Selection of Heat Disposal Methods for a Hanford Nuclear Energy Center, BNWL-2003 Battelle, Pacific Northwest Laboratories, Richland, WA, June 1976, 97 p.

8. Ramsdell, J. V., Impact of a Hanford Nuclear Energy Center on Ground Level Fog and Humidity, BNWL-2058, Battelle, Pacific Northwest Laboratories, Richland, WA, March 1977, 107 p.

9. Ramsdell, J. V. and D. I. Diebel, Meteorological Evaluation of Multiple Reactor Contamination Probabilities For a Hanford Nuclear Energy Center, PNL-2452, Battelle, Pacific Northwest Laboratories, Richland, WA, March 1978, 53 p.

10. Clark, R. G. and W. J. Dowis, Reliability of Generation at a Hanford Nuclear Energy Center (HNEC), BNWL-2474, Battelle, Pacific Northwest Laboratories, Richland, WA, 1978, 201 p.

11. Gifford, F. A., "An Outline of Theories of Diffusion in the Lower Kayers of the Atmosphere," in Meteorology and Atomic Energy-1968, D. Slade, ed., TID-24190, U.S. Atomic Energy Commission, July 1968.

12. Csanady, G. T., Turbulent Diffusion in the Environment, D. Reidell, Boston, 248 p., 1973.

13. Briggs, G. A., Plume Rise, TID-25075, U.S. Atomic Energy Commission, November 1969.

14. Briggs, G. A., "Diffusion Estimation for Small Emissions," Atmospheric Turbulence and Diffusion Laboratory 1973 Annual Report, ATDL-106, pp. 83-145, December 1974.

15. Ochs, H. T., III, "Modeling of Cumulus Initiation in METROMEX," J. Appl. Meteor., 14:873-882, 1975.

16. Junod, A., R. J. Hopkirk, D. Schneiter and D. Haschke, "Meteorological Influences of Atmospheric Cooling Systems as Projected in Switzerland," Cooling Tower Environment - 1974, CONF-740302, ERDA Symposium Series, U.S. Energy Research and Development Administration, pp. 239-264, 1975.

17. Hanna, S. R., "Predicted Climatology of Cooling Tower Plumes from Energy Centers," J. Appl. Meteor., 16:880-887, 1977.

18. Geiger, R., The Climate Near the Ground, Harvard University Press, Cambridge, 1959.

19. Matveev, L. T., Fundamentals of General Meteorology Physics of the Atmosphere, Leningrad, 1965, Translated by Israel Program for Scientific Translations, 1967.

20. Quinn, W. H. and W. V. Burt, "Computation of Incoming Solar Radiation Over the Equatorial Pacific," J. Appl. Meteor., 7:490-498, 1968.

21. Pochop, L. O., M. D. Shanklin and D. A. Horner, "Sky Cover Influence on Total Hemispheric Radiation During Daylight Hours," J. Appl. Meteor., 7:484-489, 1968.

22. Morgan, D. L., W. O. Pruitt and F. J. Lourence, "Estimation of Atmospheric Radiation," J. Appl. Meteor., 10:463-468, 1971.

23. Huang, J.C.K. and J. M. Park, "Effective Cloudiness Derived from Ocean Buoy Data," J. Appl. Meteor., 14:240-245, 1975.

24. Lund, I. A., "Methods for Estimating the Probability of Clear Lines of Sight or Sunshine Through the Atmosphere," J. Appl. Meteor., 5:625-630, 1966.

25. Quinn, W. H., W. V. Burt and W. M. Pawley, "A Study of Several Approaches to Computing Surface Insolation Over Tropical Oceans," J. Appl. Meteor., 8:205-212, 1969.

26. Lund, I. A. and M. D. Shanklin, "Photogrammetrically Determined Cloud-Free Lines of Sight Through the Atmosphere," J. Appl. Meteor., 11:773-782, 1972.

27. Angell, J. K. and J. Korshover, "Variation in Sunshine Duration Over the Contiguous United States Between 1950 and 1972," J. Appl. Meteor., 14:1174-1181, 1975.

28. Stone, W. A., D. E. Jenne and J. M. Thorp, Climatography of the Hanford Area, BNWL-1605, Battelle, Pacific Northwest Laboratories, Richland, WA, 1972.

29. List, R. J., Smithsonian Meteorological Tables, Smithsonian Institution Press, Washington, 1971.

30. Pollard, J. H., A Handbook of Numerical and Statistical Techniques, Cambridge University Press, Cambridge, 1977.

DISTRIBUTION

No. of Copies

OFFSITE

1 DOE Chicago Patent Group
A. A. Churm

1 Aluminum Company of America
Post Office Box 120
Vancouver, WA 98660
Lyman J. Harris
Northwest Area Power Manager

1 Benton County Public Utility District
Post Office Boz 6270
Kennewick, WA 99336
Robert W. Blodgett, Manager

1 Bonneville Power Administration
Post Office Box 3621
Portland, OR 97208
C. Ray Foleen
Deputy Administrator

1 Culp, Dwyer, Guterson & Grader
1300 Hoge Building
Seattle, WA 98104
Gordon Culp

1 Electric Power Research Institute
Post Office Box 10412
Palo Alto, CA 94304
Laura Henning

20 Department of Energy
Mail Stop F-309
Washington, DC 20545
W. F. Savage, Chief
Advanced Concepts Evaluation Branch

No. of
Copies

OFFSITE

27 DOE Technical Information Center

1 Nuclear Regulatory Commission
Washington, DC 20555

1 Pacific Northwest Utilities Conference Committee
Post Office Box 1231
Wenatchee, WA 98801

Howard C. Elmore, Chairman

1 Pacific Northwest Utilities Conference Committee on Engineering and Planning
2730 Northwest 77th Place
Portland, OR 97213

David J. Lewis, Consultant

1 Portland General Electric Company
621 Southwest Alder Street
Portland, OR 97205

A. J. Porter, Vice President

1 Puget Sound Power and Light Company
Puget Power Building
Post Office Box 535
Bellevue, WA 98004

John W. Ellis, President

1 Jack Criswell, General Manager
Springfield Utility Board
250 North "A" Street, Box 300
Springfield, OR 97477

1 National Academy of Public Administration
1225 Connecticut Avenue NW
Washington, DC 20036

R. Kloman

1 Washington State Energy Office
1000 South Cherry
Olympia, WA 98504

Larry Bradley

No. of
Copies

OFFSITE

1 Western Interstate Energy Board/WINB
2500 Stapleton Plaza
3333 Quebec
Denver, CO 80207

John L. Watson, Executive Director

1 South Carolina Energy Research Institute
Suite 670, First National Bank Building
Main at Washington
Columbia, SC 29201

John Sharp

1 Oak Ridge National Laboratory
Post Office Box X
Oak Ridge, TN 37830

Tom Cole

1 Southern Interstate Nuclear Board
One Exchange Place
Suite 1230
Atlanta, GA 30341

Scott Fellows

1 U.S. Nuclear Regulatory Commission
Mail Stop 7609 MNBB
Washington, DC 20555

R. T. Jaske

1 Battelle Southern Services
101 Marietta Tower
Suite 3313
Atlanta, GA 30303

Barry Benator

15 Energy Facility Site Evaluation
820 East Fifth Avenue
Olympia, WA 98504

W. L. Fitch

No. of
Copies

ONSITE

8 DOE Richland Operations Office

W. A. Burns
O. J. Elgert
P. W. Gottschalk
R. H. Lindsey/G. L. Liffick
H. E. Ransom
F. R. Standerfer
M. W. Tiernan

34 Pacific Northwest Laboratory

D. B. Cearlock
R. L. Conley
D. W. Dragnich
R. F. Foster
J. J. Fuquay
H. Harty (5)
J. V. Ramsdell (10)
A. E. Reisenauer
W. H. Rickard
C. L. Simpson
J. K. Soldat
R. W. Wallace
D. G. Watson
Technical Information (5)
Publishing Coordination (2)

2 Washington Public Power Supply System

Rodger K. Woodruff
J. R. Young